Construction of a Gridded Energy Analyzer for Measurements of Ion Energy Distribution in the Versatile Toroidal Facility

by

Shaun L. Meredith

B.S. Nuclear Engineering
Massachusetts Institute of Technology, 1990

SUBMITTED TO THE DEPARTMENT OF NUCLEAR ENGINEERING IN PARTIAL FULFILLMENT OF THE REQUIREMENTS FOR THE DEGREE OF

MASTER OF SCIENCE IN NUCLEAR ENGINEERING
AT THE
MASSACHUSETTS INSTITUTE OF TECHNOLOGY

JUNE 1998

Signature of Author: _____
Department of Nuclear Engineering
May 8, 1998

Certified by: _____
Prof. Min-Chang Lee
Thesis Supervisor

Certified by: _____
Prof. Ian Hutchinson
Thesis Reader

Accepted by: _____
Prof. Lawrence Lidsky
Chairman, Departmental Committee on Graduate Students

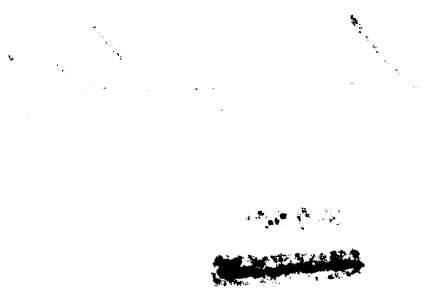

Construction of a Gridded Energy Analyzer for Measurements of Ion Energy Distribution in the Versatile Toroidal Facility

by

Shaun L. Meredith

Submitted to the Department of Nuclear Engineering on May 8, 1998 in Partial Fulfillment of the Requirements for the Degree of Master of Science in Nuclear Engineering

ABSTRACT

The Versatile Toroidal Facility (VTF) at MIT's Plasma Science and Fusion Center provides a laboratory environment for studying ionospheric plasmas. Various plasma diagnostic devices have been created and used to study the VTF plasma since 1991. An accurate method for measuring VTF's ion characteristics has never been designed or installed in the laboratory facility. Gridded Energy Analyzers (GEA) are useful diagnostic tools for determining plasma ion energy distributions and ion temperature. Research was done on the theory behind Gridded Energy Analyzers and their applicability for use in the Versatile Toroidal Facility. A design and method for constructing a miniaturized GEA for VTF was developed and documented. The construction method covers material selection, machining, and assembly of VTF's miniature GEA. The miniature GEA is a non-perturbing probe used in VTF's plasma, which is approximately 3 cm in diameter. The GEA was constructed and preliminary experimental data was obtained. From this data VTF's ion temperature was found to be approximately 8eV and an ion distribution function was determined to be roughly Maxwellian in nature.

Thesis Supervisor: Prof. Min-Chang Lee
Title: Head of Ionospheric Plasma Research Group, Plasma Science and Fusion Center

Thesis Reader: Prof. Ian Hutchinson
Title: Head, Alcator Project, Plasma Science and Fusion Center

Acknowledgments

I would like to thank Professor Min-Chang Lee for his supervision and support in all the phases of my research. Professor Lee provided me with the guidance to complete this work in an extremely tight time schedule, along with the opportunity to work with the Versatile Toroidal Facility (VTF) group at MIT. I would also like to thank Professor Lee for the concern he has shown for myself and his other students working on the VTF project. He consistently shared his great knowledge and enthusiasm with his students while providing them with encouragement to seek out new research areas.

I would also like to thank my fellow students at VTF. Without the work and support of Kevin O'Donnell, Nathan Dalrymple, Ryan Riddolls, Mike Rowlands, Piotr Jastremski, and Mike Starks I would have never accumulated enough knowledge to finish the construction of the GEA. It was a pleasure to work in such a friendly environment.

I would also like to thank Dr. Bill Burke of Phillips Laboratory. His discussions with me proved to be incredibly enlightening as to the complexity and wonders of plasma physics. I will miss working with each and every one of the people mentioned above.

Contents

List of Figures

List of Tables

1. Introduction

1.1 Motivation

The microscopic properties of plasmas can be described by one basic function, the distribution function. Macroscopic properties, such as density, temperature, and transport properties, can all be derived from the distribution function. Kinetic instabilities and their saturation properties via wave particle interactions can be examined with the shape of the distribution function. In spite of the importance of the distribution function, $f(\mathbf{r},\mathbf{v},t)$, one finds suprisingly few direct measurements of $f(\mathbf{r},\mathbf{v},t)$ in laboratory plasmas. Such is the case at the Versatile Toroidal Facility (VTF) at MIT's Plasma Science and Fusion Center. The VTF experiment is used to simulate ionospheric plasma conditions in the laboratory. With the exception of a short lived gridded energy analyzer installed and removed in 1995, VTF has not had the ability to directly measure distribution functions in the plasma.

The main focus of VTF's research over the last several years has been to conduct joint field experiments in Arecibo, Puerto Rico and laboratory experiments in the VTF regarding plasma wave processes in the ionosphere. Parametric decay, resonant absorption, and anomalous microwave absorption are a few processes that have been studied in both the ionosphere and VTF (Riddolls et al., 1995 and Riddolls, 1996). Parametric decay in overdense plasmas and scattering of Langmuir waves by lower hybrid waves are topics of study (Lee et al., 1997). Particle precipitation and other current-driven phenomena such as those found naturally in the auroral electrojet contain similarities with those found in the beam plasmas of VTF. In fact, combined wave and particle measurements provide an ideal way to study wave-

particle interactions. In order to study these events more closely it is a natural extension to produce a diagnostic to accomplish the task.

The existence of VTF as an accessible and efficient laboratory to study ionospheric plasma physics attracts the interest of radio scientists and space physicists. Thus, the motivation for the efforts to produce a plasma diagnostic for VTF, which can measure ion distribution functions directly.

1.2 Outline

This thesis begins with an introduction to the laboratory facility, VTF. This laboratory consists of a toroidal vacuum vessel and magnetic field coils weighing over thirty tons. Power systems in the megawatt range provide power to the toroidal and vertical field magnets and the plasma beam system filaments. Computerized controls allow for the safe operation of the facility.

Section 3 begins with an introduction to the theory of Langmuir probes followed closely with a discussion of how the theory applies to the concept of a gridded energy analyzer. A simplified gridded energy analyzer (GEA) is presented and the benefits of a more refined design with multiple grids are discussed. The multiple grid analyzer concept is selected for implementation in the VTF.

Section 4 covers materials selection for the probe assembly. Constructing a probe which could withstand constant bombardment from high energy particles requires materials which can accept a large heat loading. To prevent disrupting the plasma flow the probe had to also be designed to be as compact as possible. This

miniature probe would allow for other diagnostics placed downstream in the plasma not to be located in the GEA's "shadow".

Preliminary measurements for testing the operation of the miniature GEA are presented in Section 5. An ion distribution function was found for several radii in the VTF. In addition, ion temperature was determined for VTF.

This thesis concludes with Section 6 where a few recommendations for future work with the GEA are offered.

2. Experimental Apparatus

In 1989 Professors Min-Chang Lee and Ronald Parker proposed that a large plasma experiment be constructed at MIT's Plasma Science and Fusion Center to simulate the ionospheric plasma conditions in a laboratory experiment. The Versatile Toroidal Facility, VTF as it became known, was built starting in the summer of 1989. The device had a very slim budget and much of the construction was made possible through the donation of materials from discontinued fusion projects.

The construction was made possible through the sponsorship of the Air Force Office of Scientific Research and the MIT Undergraduate Research Opportunities Program. The main toroidal field magnets, poloidal field supports, and the power supplies were provided from discontinued fusion programs, namely the Oak Ridge ISX-B machine and the MIT Tara Tandem Mirror Machine. The construction was completed by over thirty undergraduate and graduate students and VTF produced its first plasma on New Year's Eve 1990.

The next summer a Langmuir Probe was installed followed by a radially scanning RF antenna. Then the characterization of VTF began. Since then several diagnostics have been installed and removed as the plasma was characterized further. Such instruments have included Langmuir probes, potential probes, dipole antennas, loop antennas, and a gridded energy analyzer.

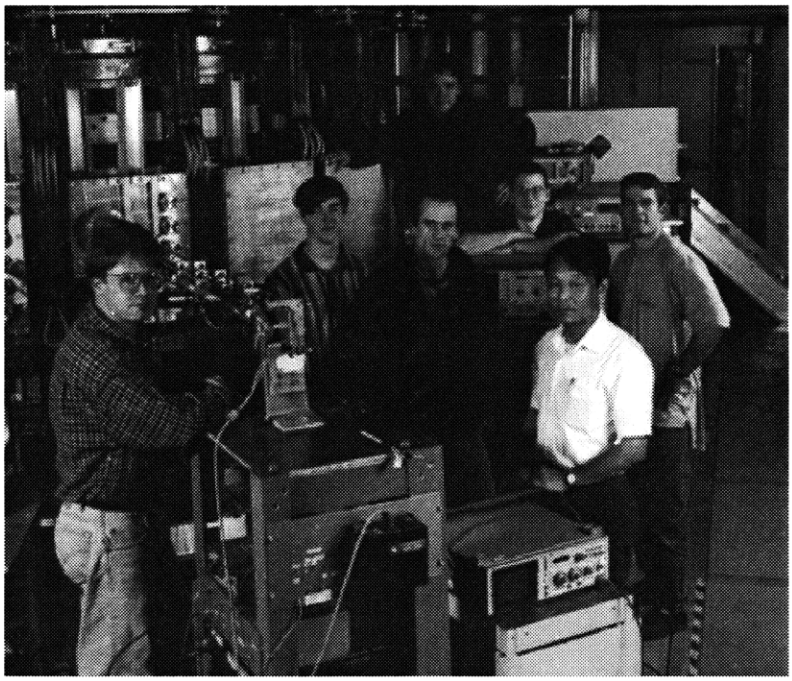

Figure 1. Versatile Toroidal Facility, June 1996

Versatile Toroidal Facility is located in the west wing of the MIT Plasma Science and Fusion Center. Figure 1 shows the facility and some of the VTF group members during the summer of 1996. The device itself consists of an integrated system with inputs, outputs, and interlocks being monitored hundreds of times a second, yet can be controlled by one person at a single console. The device is operated from a control room located adjacent to the cell where the device is housed. Two students are required for operation due to safety requirements.

Major Radius	0.9 m
Minor Radius	0.3 m
Toroidal Field	1800 G
Vertical Field	10-20 G
Electron Density	10^{10}-10^{13} cm^{-3}
Bulk Electron	10 eV

Table 1. Typical VTF Parameters

The device itself is a toroidal plasma device with a major radius of 0.9 m and a minor radius of 0.3 m in which ionospheric plasma interactions with injected waves and charged particle beams can be studied. A basic list of parameters for VTF can be found in Table 1. For a further description of the VTF facility see *Design and Construction of the Versatile Toroidal Facility for Laboratory Simulation of Ionospheric Plasmas* (Moriarty, 1990).

2.1 An Ionospheric Plasma Laboratory

VTF is used as a cross check for wave injection experiments at Arecibo, Puerto Rico and to support theoretical studies. It can be used for ionospheric simulation based upon the parameters shown in Table 2.

The first parameter states that the density gradient is perpendicular to the magnetic field. In the ionosphere density gradients exist both parallel and perpendicular to the Earth's magnetic field. Generally, the parallel gradient does not act as an important source for driving plasma wave instabilities in the ionosphere. The parallel gradient is omitted in comparison with the perpendicular gradient.

In the ionosphere the second parameter, $f_{pe} \geq f_{ce}$, can be a ratio as high as 8 to 1. Producing such a ratio in a lab is extremely difficult since the magnetic field is used to confine the plasma and allows high densities. To prevent arcing of the electron beam

plasma source to the vessel walls a minimal toroidal field is required. Thus, we can frequently get a ratio of approximately 3 to 1. The third and fourth parameters are dependent on each other. The high neutral pressure makes for high collision rate and low fractional ionization.

Ionospheric Parameters
$\nabla n \perp \vec{B}_o$
$f_{pe} \geq f_{ce}$
$2\% < \frac{n_e}{n_o} < 20\%$
$\frac{\nu_i}{\Omega_i} \sim 10^{-2}, \frac{\nu_{ei}}{\Omega_e} \sim 10^{-4}$
H, Ar, O, or N plasmas
DC $\vec{E}_o$

Table 2. Ionospheric Parameters Present in VTF

The plasmas can be made from many gases. Most often Hydrogen is used but for electron beam plasmas Argon ionizes more easily and produces high current beams.

Finally, the cathodes produce parallel electric fields and strong perpendicular electric fields similar to those produced by neutral winds in the ionosphere.

2.2 Magnets

The magnet system originated from Oak Ridge National Laboratory's ISX-B experiment. After it was decommissioned the toroidal field magnets, bucking cylinder, and torque cylinders were used for creating VTF.

The eighteen toroidal field magnets are placed around the vacuum vessel and secured in place by the bucking cylinder. Each copper magnet has four turns that are insulated and epoxied together. The bucking cylinder prevents radial motion inward. The vacuum vessel and the torque cylinders provide support against the toppling force created by the vertical field coils. The toroidal field coils have the ability to be water cooled but are presently air cooled. Under normal operation with a magnetic field of 1000-1800 Gauss the magnets remain at room temperature.

A weaker vertical field is produced by a set of Helmholtz coils. Generally a vertical field of approximately 10 Gauss is applied.

2.3 Vacuum System

Vacuum is maintained by two pumps operating in series. A Leybold Heraeus rotary vane Trivac roughing pump provides vacuum at approximately 1 mTorr at the turbo pump outlet. A Leybold Heraeus 500 liter per second turbomolecular pump is used to bring the vessel down to operating vacuums. Typical operating base pressure is near 2.6×10^{-7} Torr.

The vacuum vessel was built partially by Atomic Limited of Cambridge, Massachusetts and partially through students efforts. It has a major radius of 0.90 m and is roughly 6 m^3 in volume. The vessel itself and many of the other components are made of 304 stainless steel due to the low off gassing and nonmagnetic properties. The port covers are made of aluminum to reduce machining complications. However, port covers with diagnostics are commonly made of 304 stainless steel to allow

welding of standard vacuum components. There are 48 ports for easy access and a variety of probe locations.

2.4 Power Supplies

The toroidal field coils require between 500 kW and 2 MW for normal operation and each filament used for an electron beam discharge requires over 30 kW. The Tara Tandem Mirror experiment left over 10 MW of power systems when it was decommissioned.

The converters used to power the toroidal field magnets are capable of delivering 7kA at 400 Volts. Two converters are used in parallel to supply the toroidal field current. Each converter is a six pulse phase controlled rectifier using silicon controlled rectifiers. The incoming power is at 480 Volts and the circuit breakers are thermally tripped. They are capable of 7kA for approximately sixty seconds.

Power to the electron beam cathodes and the vertical field is supplied through the TARA neutral beam arc and filament supplies. Each filament supply is capable of 3kA at 20 Volts and each arc supply can handle 300 A at 375 Volts. Four supplies are dedicated to the four beam filaments. One supply's filament is used for the vertical field Helmholtz pair. The arc supplies have under voltage and over-current trips, which protect the filaments in case of arcing to the nearby vacuum vessel.

2.5 Control Systems

Two personal computers (PC) are used to control the VTF experiment. A simple diagram of the controls is shown in Figure 2. The first PC is hardwired to a CAMAC via a GPIB connection. Both the CAMAC and GPIB interface have been used

as standards in experimentation for two decades. All the engineering data and scientific diagnostic analog signals are converted to digital format by the CAMAC and stored to the PC hard disk. Typically a plasma shot runs for a few seconds and then the data is recorded to the hard drive.

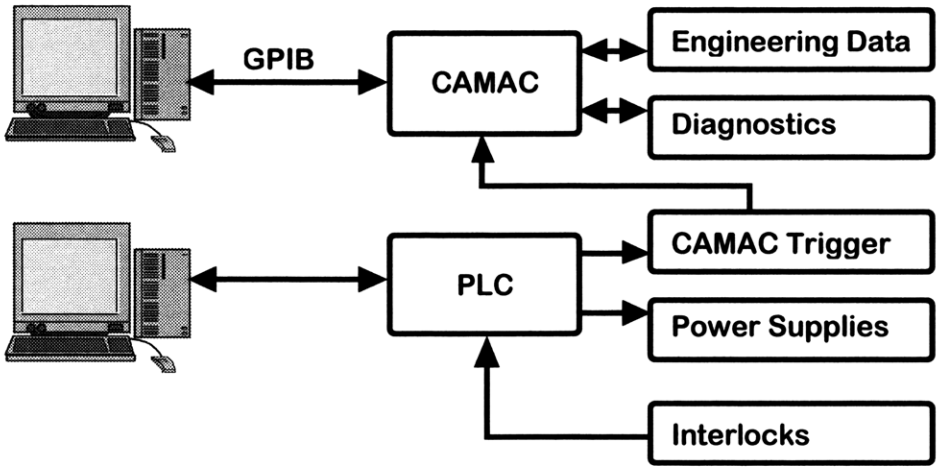

Figure 2. VTF Control Systems

The digitizers used in the CAMAC crates are LeCroy 8212 A/D converters and 8800 memory modules are used for data capture. The digitizers are capable of up to 32 differential inputs and convert signals at up to 160kHz at 12 bit resolution. Engineering signals are typically digitized at 1 ksample/sec for eight seconds. Physics signals are digitized at approximately 10 ksamples/sec. For better time resolution some signals are digitized by LeCroy 2264 A/D converters. These have a resolution of 8 bits but can run at 4Mhz.

Communication with the CAMAC is performed in the LabWindows environment, which is programmed in QBASIC. Often LabWindows does not provide a sufficient environment for data analysis therefore signal processing and data analysis is often performed in MatLab.

The second PC uses a Paragon user interface to control the Allen Bradley Programmable Logic Controller (PLC). The PLC controls the power supplies, monitors the safety interlocks, and controls other signals necessary for the automated operation of VTF. The experimenter has the capability of enabling/disabling power supplies, enabling/disabling diagnostics, programming power levels, setting turn on/off times for various devices, and monitoring cell security.

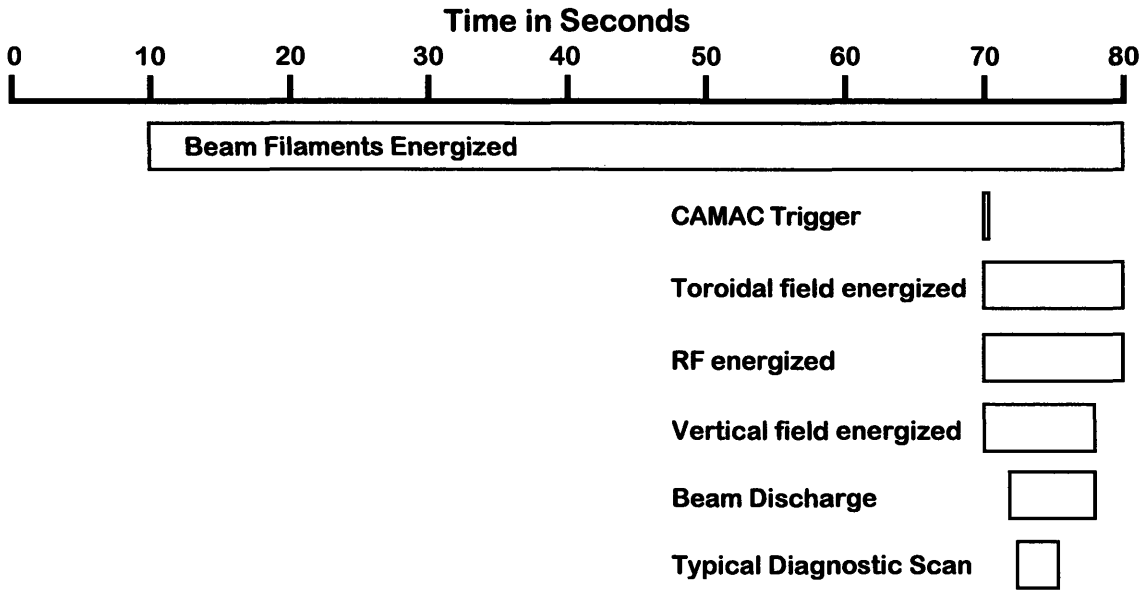

Figure 3. Typical Plasma Shot Sequence

Timing of the experiments vary somewhat from plasma shot to plasma shot depending on the experimenter. Figure 3 shows the timing sequence for a typical plasma shot. Ten seconds is required for the PLC to calculate set points and sound a warning klaxon in the cell. At ten seconds into the process the beam filament are turned on to begin heating. This next sixty seconds can be eliminated for an RF generated plasma (See **Section 2.6 Plasma Sources**). Seventy seconds into the cycle the CAMAC is triggered by the PLC to allow engineering and control signals to be recorded. In addition, the toroidal field and vertical field coils are turned on and RF is

injected. After allowing two seconds for the vertical field coils to energize the beam arc supplies are powered. Data is then recorded after the beams have had one second to settle into a "steady state". Typical plasma shots have a data recording time of three seconds.

2.6 Plasma Sources

Plasma may be produced in the VTF by one of three sources: radio frequency (RF), hot cathode beam injection, and Taylor discharge. The third plasma source is currently out of commission but work is ongoing to bring it back into service. In addition to using each of the sources independently, RF and beam plasma discharges (BPD) can be used in conjunction with each other to produce a plasma similar to the auroral ionospheric plasma.

The BPD system consists of four LaB_6 cathodes and four biasing power supplies. The cathodes can be used in any combination and from one to four can be turned on at once. Each cathode is heated ohmically for sixty seconds by a twenty volt 2000 A floating power supply delivering 500 A. A helical magnetic field is then applied in the vacuum vessel and an arc bias of -150 to -375 Volts is applied to each cathode. The potential ejects energetic electrons from the cathode, which allows them to be trapped by the magnetic field. The electrons flow along the magnetic field and collide with neutrals initiating the discharge. Typical beam plasmas produce a 50 A per beam current with a plasma density of $5x10^{11}$ cm^{-3} having electron temperatures of 8 to 10 eV.

Magnetic field strength is varied in the toroidal and vertical directions to maintain the desired helical structure. In this manner the diagnostics location in the plasma stream can be changed without changing the location of the probes. When multiple beams are used the toroidal field must be increased to prevent the plasma from arcing to the vacuum vessel walls.

Following a vacuum break, the cathodes must be biased with low voltages and increased in small increments to the normal operating voltage of 12 Volts. This "conditions" the cathodes by allowing impurities that were absorbed during atmospheric contact to outgas. If this procedure is not followed, the gas pressure inside the LaB_6 will cause them to shatter. In addition to this conditioning several plasma shots must be made before achieving a clean plasma. Oxide layers form on the cathodes causing frequent arcing to the vacuum chamber and erratic beam currents.

The cathodes deteriorate in the sense that the ceramic collects carbon dust from the nearby carbon structures around the cathodes. When the cathodes emit consistent steady beams they essentially clean themselves which extends the time between maintenance cycles. This was much more of a problem before a modification was made in January of 1997 which replaced much of the carbon with stainless steel. If maintenance is required the cleaning process leaves many impurities in the ceramic which results in months of operation before the cathode beams produce a clean plasma.

The Radio Frequency produced plasma is rather straightforward. A Gerling Labs 3kW magnetron power supply and control unit provide the wave power. A

WR384 waveguide is connected to the magnetron and the power is launched into the plasma after passing through a protective circulator, a bi-directional coupler, a DC break, a ceramic vacuum window, and a horn. The injected power reacts with the gas leaked into the chamber to break down and sustain a plasma.

The protective circulator insulates the magnetron from reflected power from the waveguide interfaces. The coupler provides a sample of the forward and reflected power at 55.6 dB below the level in the waveguide. The signal can then be sent to a spectrum analyzer to record the injected or reflected spectrum. The DC break is used to isolate grounds and the ceramic window provides a vacuum feedthrough for the RF. The launching horn measures ten by twelve inches and was installed to stop large power reflections (~40%) back through the opening. This horn was designed to couple with the plasma and provides low reflected power (~3%). The port opening physical constraints restricted a further reduction in the reflected power.

By varying the toroidal and vertical fields a variety of plasma density profiles can be obtained (Moriarty, 1996). With 3kW of ECRH power launched into the vessel densities of up to $7x10^{10}$ cm^{-3} and temperatures of approximately 5 eV have been produced. A weak vertical field (~10 Gauss) can enhance the density by about 50% but a stronger vertical field can reduce the profile's peak density. A comparison of O-mode versus X-mode launched power showed O-mode to be about 50% more dense for similar magnetic fields (Moriarty, 1996).

3. Theory

3.1 Langmuir Probe Theory

In order to understand the theory behind the operation of a GEA one needs a comprehension of electrostatic probes often referred to as Langmuir probes. When a probe is placed in a plasma the potential difference between the probe and the plasma is mainly confined to a "sheath region" which is generally a few Debye lengths thick.

A planar approximation is used in developing the equations used for diagnostic purposes since the probe sheath is small and the equations would prove to be complicated otherwise. Since sheath thickness is small compared to the probe size an approximation that probe surface area can be used for sheath surface area can be made (Hutchinson, 1987).

The following assumptions are made for this analysis:

- probe dimensions are large compared to the Debye length (VTF's Debye Length is about 0.1 mm and the probe tip is about 3.2 mm)
- ions in the plasma start far away from the probe with negligible energy
- probe dimensions are small relative to the mean free path (VTF's mean free path is on the order of 2 m)

A metal probe inserted in a plasma will draw a current that depends on the applied potential, the plasma temperature, density, species, and the plasma reference potential. Careful interpretation of the results is required because the presence of the probe can alter local plasma conditions. Measurement of the I-V characteristic of the

probe will yield electron temperature, T_e, electron density, n_e, floating potential, V_f, and plasma reference potential, V_p. Below is the theory that enables the interpretation of the results.

The current for singly-charged ions leaving a probe of surface area, A, is

$$I = -Ae(n_i v_i - n_e v_e)$$

where

n_i = ion density
n_e = electron density
v_i = ion velocity towards the probe
v_e = electron velocity towards the probe

For a Maxwellian distribution (using a one dimensional approach),

$$\sigma_e(x) = -e\int_{-v_o}^{\infty} f_e dv$$

$$J_e = -e\int_{-v_o}^{\infty} v f_e dv$$

where

σ_e = electron charge density
x = distance from the probe
J_e = current density

$$v_o = \sqrt{\frac{2e}{m_e}(\phi - \phi_o)}$$

ϕ = potential in sheath region near the probe
ϕ_o = potential of probe with respect to the bulk plasma

$$f_e = n_o\left(\frac{m_e}{2\pi T_e}\right)^{\frac{1}{2}} \exp\left(\frac{-m_e v^2}{2T_e} + \frac{e\phi}{T_e}\right)$$

n_o = density far from probe

$$\sigma_e(x) = -en_o\left(\frac{m_e}{2\pi T_e}\right)^{\frac{1}{2}} \exp\left(\frac{e\phi}{T_e}\right)\int_{-v_o}^{\infty} \exp\left(\frac{-m_e v^2}{2T_e}\right)dv$$

$$\sigma_e(x) = -en_o \exp\left(\frac{e\phi}{T_e}\right) \text{since } e\phi >> T_e$$

$$J_e(x) = -en_o\left(\frac{m_e}{2\pi T_e}\right)^{\frac{1}{2}} \exp\left(\frac{e\phi}{T_e}\right)\int_{-v_o}^{\infty} v\exp\left(\frac{-m_e v^2}{2T_e}\right)dv$$

Since J_e is constant, choose x in the bulk plasma where ϕ =0.

$$J_e = -en_o\left(\frac{T_e}{2\pi m_e}\right)^{\frac{1}{2}} \exp\left(\frac{e\phi}{T_e}\right)$$

Next we divide space into two regions, Region I where the Ions are accelerated to sonic velocity in quasineutral space and Region II or the sheath region where Poisson's equation must be solved.

Each ion enters the sheath region at velocity v_s. Then, conservation of energy yields

$$\frac{1}{2}m_i v_i^2 + e\phi = e\phi_s + \frac{1}{2}m_i v_s^2$$

But the ions started deep in the plasma with no energy so the left hand side is set to zero leaving

$$v_i = \sqrt{-\frac{2e\phi}{m_i}}$$

Now

$$\sigma_i = \frac{J_i}{v_i} = \frac{J_i}{\sqrt{-\frac{2e\phi}{m_i}}}$$

Solving Poisson's equation:

$$\frac{d^2\phi}{dx^2} = -\frac{1}{\varepsilon_o}(\sigma_i - \sigma_e) = -\frac{1}{\varepsilon_o}\left(\frac{J_i}{\sqrt{-\frac{2e\phi}{m_i}}} - en_o \exp\left(\frac{e\phi}{T_e}\right)\right)$$

It can be shown that to match regions I and II, ions must enter the sheath at the acoustic velocity (Chen, 1984)

$$v_s = \sqrt{\frac{T_e}{m_i}}$$

then,

$$\phi_s = -\frac{m_i v_s^2}{2e} = -\frac{m_i}{2e}\frac{T_e}{m_i} = -\frac{T_e}{2e}$$

Since $n_e \approx n_i$ at the boundary,

$$\frac{J_i}{\sqrt{-\frac{2e\phi_s}{m_i}}} = en_o \exp\left(\frac{e\phi}{T_e}\right)$$

$$J_i = en_o\sqrt{-\frac{2e}{m_i}\left(\frac{-T_e}{2e}\right)}\exp\left(\frac{e}{T_e}\left(-\frac{T_e}{2e}\right)\right)$$

$$J_i = en_o\sqrt{\frac{T_e}{m_i}}\exp\left(-\frac{1}{2}\right) \cong 0.61en_o\sqrt{\frac{T_e}{m_i}}$$

Then the current is calculated as

$$I = -A(J_i + J_e) = Aen_o\left\{\left(\frac{T_e}{2\pi m_e}\right)^{\frac{1}{2}} \exp\left(\frac{e\phi}{T_e}\right) - 0.61\left(\frac{T_e}{m_i}\right)^{\frac{1}{2}}\right\}$$

An exact solution of the three dimensional Poisson equation in the sheath region yields a coefficient of 0.54 instead of 0.61 (Bohm et al, 1949). From here on we will use the coefficient presented by Bohm.

Now we let V_p= plasma potential with respect to the chamber ground. Realizing for an open circuit, I=0, and setting the open circuit voltage to V_f, known as the floating potential, we get,

$$V_f = V_p + \frac{T_e}{2e}\left(\ln\frac{m_e}{m_i} + 0.54\right) \qquad \textit{Equation 1}$$

If we make ϕ_o sufficiently negative that the electron contribution is negligible, we get a limit on the current called the ion saturation current, I_{si}.

$$I_{si} = -Aen_o(0.54)\left(\frac{T_e}{m_i}\right)^{\frac{1}{2}} \qquad \textit{Equation 2}$$

We can obtain T_e by taking the derivative, dI/dV

$$\frac{dI}{dV} = Aen_o\left(\frac{T_e}{2\pi m_e}\right)^{\frac{1}{2}} \frac{e}{T_e} Exp\left(\frac{e\phi}{T_e}\right)$$

$$\Rightarrow T_e = \frac{e(I - I_{si})}{\frac{dI}{dV}} \qquad \textit{Equation 3}$$

Since it is quite difficult to find the tangent of a noisy curve trace we can use the following approach as an alternative,

$$I - I_{si} = Aen_o\sqrt{\frac{T_e}{2\pi m_e}}\exp\left(\frac{e\phi}{T_e}\right)$$

$$\frac{1}{e}\ln(I - I_{si}) = \frac{1}{T_e}\phi + \frac{1}{e}\ln\left(Aen_o\sqrt{\frac{T_e}{2\pi m_e}}\right) \qquad \textit{Equation 4}$$

So, The following procedure can then be used:

- measure the I-V characteristic
- from the slope using a least squares fit get T_e using Equation 4
- from I_{si} and T_e get n_o from Equation 2
- from the zero crossing the floating potential, V_f, can be determined
- Using Equation 1 get V_p using V_f and T_e

We can check the values of n_o obtained. V_p corresponds to the plasma potential with no probe present. If the probe is biased with a voltage, V_p, no sheath develops and the plasma is quasineutral and unperturbed for our purposes up to the probe's surface. The potential, ϕ, is zero everywhere. Then J_e corresponds to the flux of electrons with half a Maxwellian distribution.

$$J_e = -en_o\left(\frac{T_e}{2\pi m_e}\right)^{\frac{1}{2}}$$

$$I_{si} = -AJ_e = Aen_o\left(\frac{T_e}{2\pi m_e}\right)^{\frac{1}{2}}$$

We can approximate the electron saturation current as the value of I corresponding to voltage, V_p.

Thus far the effects of a magnetic field, such as the one generated in VTF, have been ignored. The main effect of this field is that the ions and electrons no longer move freely but gyrate around the magnetic field lines. The radius of their gyration is the Larmor radius, ρ, given by,

$$\rho = \frac{mv_{\perp}}{eB}.$$

If $\rho >> a$, where a is the typical probe dimension, then the previous discussion would apply. In the VTF case we can calculate the ion larmor radius, ρ_i, to be approximately 2.5 mm. For the characteristic dimension, a, the radius of the entrance to the probe, 1.14 mm, is used. An argument can be made to disregard the magnetic field effects since the probe entrance is sufficiently small and the effects of the magnetic field will be small. However, the effects of the magnetic field may be important because it is also reasonable to see that a factor of two might not be sufficient to meet the above criteria. When the magnetic field is sufficiently strong such that $\rho_i < a$, modifications to the ion collection can occur and a satisfactory theory has not been established (Hutchinson, 1987). Hutchinson discusses a quasicollisionless theory and a collisional theory. The quasicollisional theory can be used because the ion mean free path along the magnetic field is much greater than the length of the presheath region (Hutchinson, 1987). The results that are of interest yield a correction to the coefficient presented earlier so that

$$I_{si} = -Aen_o(0.49)\left(\frac{T_e}{m_i}\right)^{\frac{1}{2}}.$$

Often the coefficient is just taken as $\frac{1}{2}$ since the analysis is only accurate to about 20% anyway. This is the result that will be used although the correction to the nonmagnetized theory presented is small.

Another correction that arises is that the projection of the probe surface in the direction of the field should be used instead of the probe area; however, the GEA has a disk shaped tip so the projection is equal to the original area.

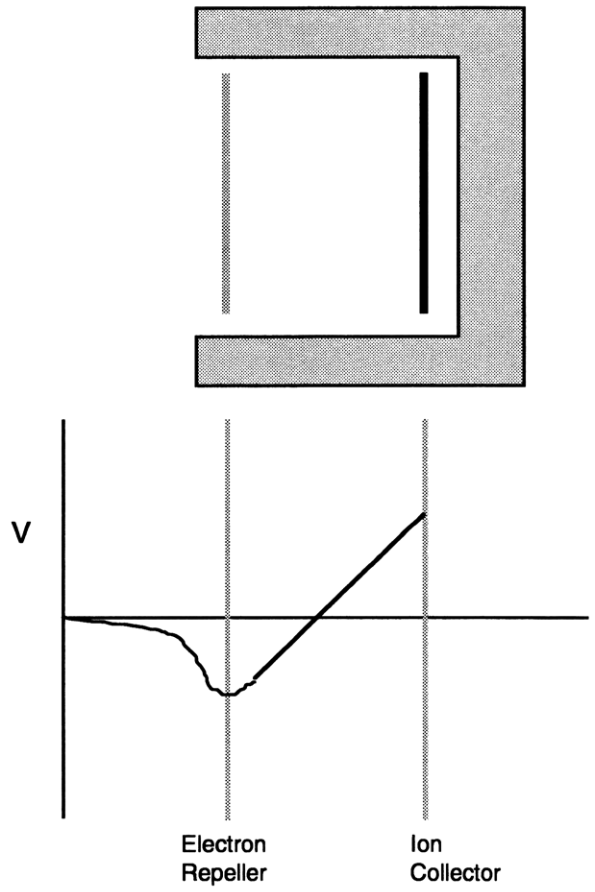

Figure 4. Simple Gridded Energy Analyzer

3.2 Application to Gridded Energy Analyzers

As can be seen from Section 3.1, when $T_i < T_e$ the Langmuir probe current is rather insensitive to ion temperature. Although some claim to measure ion temperature with a Langmuir Probe ambiguity in the constants used prohibit accurate measurements (Yang et al, 1994). That is where a gridded energy analyzer can be of use. The Langmuir probe cannot easily obtain ion distribution measurements due to the large electron saturation current it draws when at a positive potential.

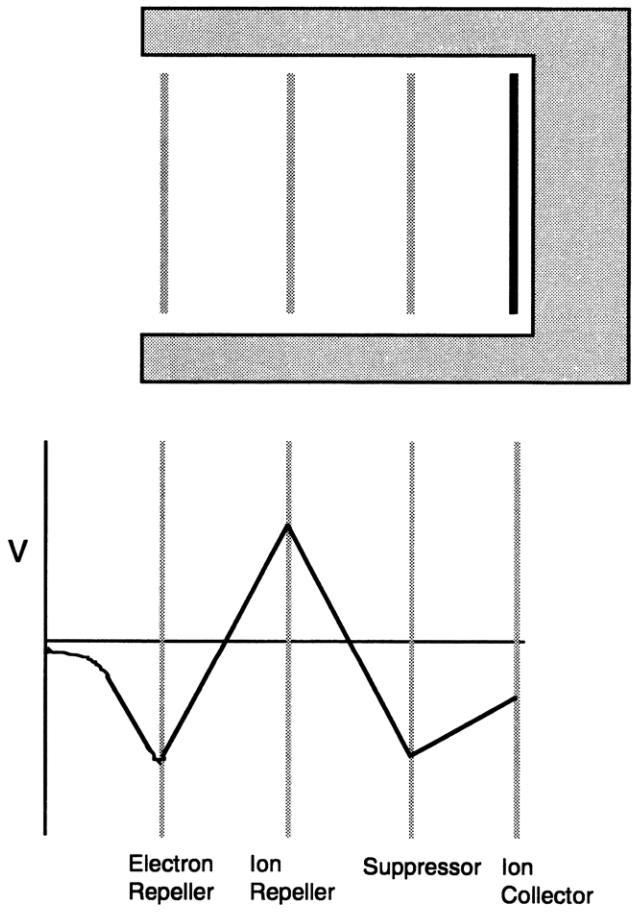

Figure 5. Suppressing Gridded Energy Analyzer

A solution to this dilemma is to use a gridded energy analyzer. A simple representation is shown in Figure 4. The plasma is allowed to approach the collector

only after passing through a grid. This grid is biased strongly negative to repel all the electrons. Then the collector voltage is varied so that only ions with energy greater than eV_c will be collected. This allows the logarithmic slope of the collected current to give the ion temperature.

The drawback of using a single grid is seen when we take into account secondary electron emissions from ions impinging on the grid. This problem can be accounted for by using the setup shown in Figure 5.

In this gridded energy analyzer (which is the simplified diagram of the approach chosen to use in VTF), the first grid repels the electrons in the bulk of the plasma. The second grid is varied to allow ions of different energies to pass through to the collector and the third grid is biased negative again to repel secondary electrons. Finally, the collector is given a small negative bias to ensure good ion collection.

Another problem with gridded energy analyzers is the limitation caused by space-charge. When the plasma enters the analyzer additional charges are placed between the grids causing changes in the potential. This change can be a problem if the potential between two grids is greater or lesser than the larger or smaller of the two grid potentials, respectively. The ions or electrons would then encounter a repelling potential hill greater than the hill given by the grids alone. If this happens then the result will be a lowering of the current of the species in question.

We can see that this worst case scenario can occur between the ion and electron repellers when the bulk of the ions have just enough energy to reach the ion repeller.

This occurs when the potential has zero slope at the ion repeller, which we can see in the discussion in Section 3.1. This is equivalent to the sheath solution when $V_s=0$. Thus we get an approximate result of (Hutchinson, 1987)

$$\frac{x}{\lambda_D} = \frac{2}{3}\left[2e^1\right]^{\frac{1}{4}}\left(\frac{eV}{T_e}\right)^{\frac{3}{4}} \cong 1.02\left(\frac{eV}{T_e}\right)^{\frac{3}{4}} \quad \textit{Equation 5}$$

Therefore, when we examine VTF's plasma parameters, the distance between grids, x, must be less than ~0.4 mm. This is very difficult to manufacture but not impossible.

4. Construction

This section starts out with an overview of the design considerations in making the miniature gridded energy analyzer. Next the materials selected are explained in relation to the design factors followed by an in depth discussion of how to manufacture the energy analyzer.

The electrical systems and the computer interface are then discussed with a follow on section detailing how to operate the analyzer with the VTF operations. The operation section is needed due to the computer interface with the probe being somewhat different than the standard VTF diagnostics.

The main purpose of this section is to give a blueprint so that another student could easily manufacture a similar probe and perhaps make some improvements in the performance. Many details were learned while building this probe which could

aid another researcher when machining a similar project. It is for that reason that this section is included.

4.1 Design Considerations

There are several factors that had to be considered in the design of the miniature GEA. The more complex issues were of size and energy deposition.

A GEA installed in VTF in 1995 (Moriarty, 1996) compensated for the space charge limit by placing a aperture before the probe to effectively reduce the density in the probe which increased the minimum spacing. This creates an unknown error in the plasma in the manifestation of total effective collection area. In addition, the previous probe was of the simple type as shown in Figure 4.

It is these limits that the miniature GEA design has focused on. The probe is designed to be a non-perturbing probe by limiting the size of the probe tip to approximately 5 mm. The miniature GEA also features a series of grids designed to reduce the secondary electron emissions from interfering with the measurement at the collector. The design is based upon the suppressing gridded energy analyzer shown in Figure 5. The space charge limitation is being addressed by placing thin mica sheets between the grids which should result in a spacing of 0.12 mm. The probe's initial entry grid is also formed from two layers of mesh. This reduces the transparency and lowers the density of the plasma within the grid chamber.

Energy is deposited into the probe resulting in elevated temperatures and possible melting. VTF's previous GEA was short lived due to the entry grid material near the aperture sputtering off when the plasma was introduced. Thus, extreme care

was taken during the materials selection process to ensure heat buildup did not cause failure.

4.2 Materials Selection

Materials selection for the probe tip was difficult due to the many different constraints encountered. There was the heat deposition problem that was mentioned in the previous section and electrical requirements that factored into the decisions along with the difficulties in machining the various materials. The grids themselves needed to be small and compact yet able to withstand the high temperatures of the plasma. Tungsten was chosen as the material to form the grids out of due to its ability to be woven into a mesh and its capacity to withstand high temperatures. The first grid, which will absorb the most energy, actually consists of two meshes fit snugly against each other. Both grids are 0.025 mm in thickness and the first is 98.4 lines per cm (lpc) while the second is 59.1 lpc. This method reduces the plasma density throughout the rest of the probe tip since it results in a transparency of 42.92%. This method was chosen over a single mesh of 98.4 lpc based on the transparency reduction from 56.25% in the single grid case and the added material, which provides a larger heat sink. The reduction in transparency aids the probe by reducing the plasma density inside the probe, although only by about ten percent, placing the probe further from the space-charge limit. The main effect is the addition of extra material. Although this results in an increased surface area for heat transfer, the extra heat capacity offsets this effect resulting in a lower peak temperature. In addition, the second grid aids in providing support against deformation that may be caused when the entrance grid is weakened at high temperatures.

To determine whether the mesh would fail when subjected to the plasma a rough lumped capacity calculation can be used. Using the properties of tungsten outlined in Table 3 and using the assumption that all the particles striking the mesh give up all their energy to the mesh we see the following.

$$\Delta T \approx \frac{Q - tQ_{rad}}{\rho V C_p}$$

where,

ΔT = temperature change
Q = energy deposited
Q_{rad} = approximate radiative heat loss, $\sigma A T_{ave}^4$
ρ = density
V = volume of material
C_p = specific heat of the material

The energy deposited in the mesh, Q, can be found by assuming a particle energy of 10eV, a beam current of ~50A, and an average temperature of 1850°K for radiative heat loss with a typical 3 second beam shot.

Thus,

$$Q = \frac{I_b t kT}{e}\left(\frac{A_p}{A_b}\right)(1 - T_g) \approx \frac{\left(10\frac{eV}{ion}\right)\left(1.6022x10^{-19}\frac{J}{eV}\right)(50A)(3s)}{\left(1.6022x10^{-19}\frac{C}{ion}\right)}\left(\frac{4.104x10^{-6}m^2}{7.069x10^{-4}m^2}\right)(1 - .4292) \approx 4.97J$$

where
kT = particle energy
I_b = beam current
A_p = area of probe
A_b = area of beam
T_g = grid transparency

And

$$tQ_{rad} \approx \left(5.6697x10^{-8}\frac{W}{m^{2o}K^4}\right)\left(4.104x10^{-6}m^2\right)(1-.4292)\left(1852^0K\right)^4(3s) \approx 4.69J$$

substituting into the above a rough estimate was obtained

$$\Delta T \approx \frac{Q-tQ_{rad}}{\rho VC_p} \approx \frac{(4.97-4.69J)}{\left(19350\frac{kg}{m^3}\right)\left[\left(4{,}104x10^{-6}m^2\right)(1-.4292)\left(2.54x10^{-5}m\right)\right]\left(133\frac{J}{kg^oK}\right)} \approx 1852^oK$$

Thus, we can see we are well below the melting point even with the liberal assumption of all the ion energy deposited into the mesh. The calculation was also done for a single mesh with a 56.25% transparency resulting in a ΔT of 2337 °K. Thus, the dual mesh was chosen for the increased heat capacity, which results in the entrance grid reaching a lower peak temperature for a given time and beam current. In addition, a sample mesh was placed in VTF for a two week testing period with several plasma shots fired. Upon removal and inspection the grid was found to be completely intact.

Tungsten	
density	19350 kg/m^3
approximate C_p	133 J/kg°K
melting point	3137 °K

Table 3. Properties of Tungsten.

Next, an insulator was needed to prevent electrical contact between the grids. The dielectric constant had to be high and it must have the capability of being machined into thin wafers. Mica proved to be the material of choice. Mica has long been used as a dielectric due to its ability to be cleaved into thin sheets and maintain good electrical insulation. It also has the added benefit of excellent strength under

compression which the probe tip assembly process uses (see **Section 4.3 Probe Tip Construction**). The mica used is 0.10 mm in thickness with a capability of withstanding a 500V potential difference.

Platinum wire with a diameter of 0.1 mm was chosen to carry the current from the grids due to its high conductivity and ability to deform. This malleability allows the mesh to be pressed into the wire loop creating an excellent electrical connection and a reasonably strong physical bond.

Vacuum components are stainless steel 316 for its temperature characteristic, high strength, and the low off gassing that occurs in the low vacuum of VTF. The stainless steel is also used as structural support for the ceramic components due to the ceramic's brittleness.

Electrical insulation is maintained by a four bore alumina tube and Sauereisen hi-temp ceramic paint. Teflon is also used to help support the probe in the carriage housing while electrically isolating it from the vacuum vessel.

Finally, the carriage assembly itself was machined from 2302 aluminum for its ease of machinability and wide availability.

4.3 Probe Tip Construction

As the probe is much smaller than its predecessor extreme caution must be taken during the construction process. Many of the parts are small and delicate. In addition, many surfaces are nearly inaccessible for cleaning once the probe is constructed. Since they will be exposed to vacuum it is necessary that great care be taken to maintain a high degree of cleanliness throughout the construction. Figure 6

contains an exploded diagram of the probe tip.

Manufacturing will be explained by addressing each part of the probe tip and then addressing the overall assembly.

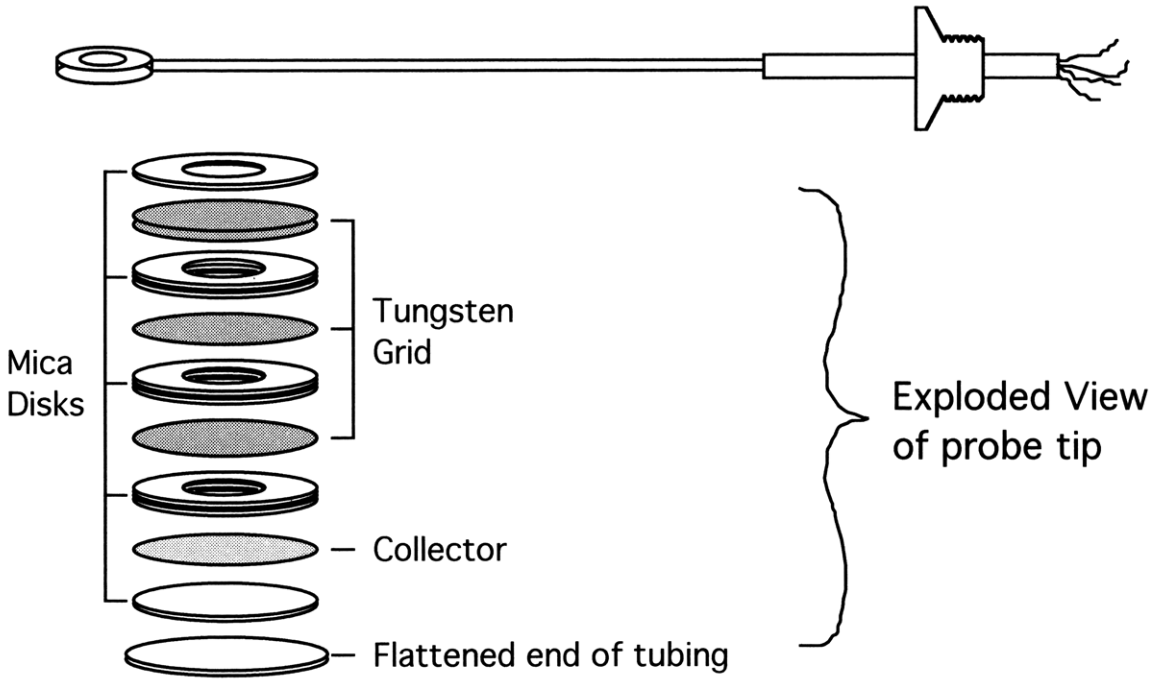

Figure 6. Exploded View of Probe Tip

The mica washers are extremely delicate and tend to crack during the machining process. For this reason it is recommended that at least three times the number of washers needed should be machined.

The procedure is as follows. First, machine two brass plates approximately 6 mm thick with tapped holes at each corner for screwing them together. Using mica sheets of 0.1 mm thickness sandwich the mica and alternate with paper layers between two brass plates and clamp the plates together with screws at the corners. Drill a small hole through the stack in the middle and then progressively use a larger

bit until a diameter of 0.228 cm is reached. Next, machine a mandrel like that shown in Figure 8 with an outer diameter equal to the inner diameter of the mica.

Do not thread the rod where the mica will rest. This will cause the mica to fracture easily on the lathe. Clamp the mica down on the mandrel taking time to

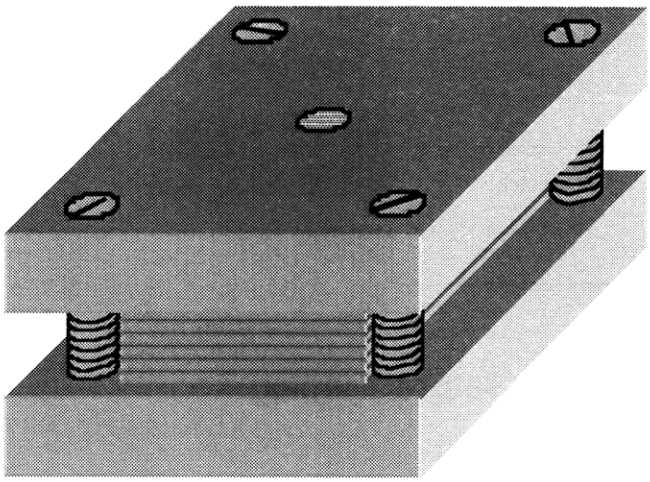

Figure 7. Sandwich the Mica disks between two plates before drilling

alternate a sheet of mica with a sheet of another material such as brass or copper. Then spin the mica disks down to an outer diameter of 0.43 cm on a lathe. The alternating of materials prevents the mica from becoming fused together when released from pressure. Mica machines well under pressure which is the reason for the mandrel and the brass plates. However, the mica also tends to form back into a solid piece when placed in compression. The paper in the first jig is sufficient to prevent the mica from fusing. The mandrel needs more support between washers and thus a more rigid material is needed to ensure the mica does not split, copper was used in this process. It is possible to get by without using another material; but, the method results in cleaving the mica into sheets after turning it down into a disk. The

cleaving process proved to be too imprecise in achieving uniform thickness washers. This completes the mica washers.

Next, a tungsten mesh consisting of 98.4 lines per cm and a line thickness of 0.0254 mm is cut to provide the grids. This mesh material was chosen to produce a grid capable of withstanding the high temperatures of the plasma. The grid also

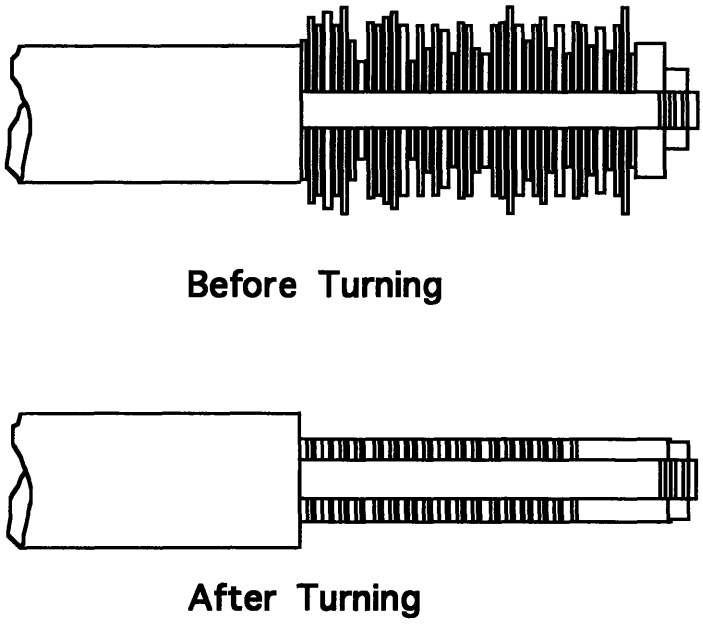

Figure 8. Mandrel for Mica Washers

provides a 93.75% transparency to the plasma, which minimizes secondary electron emissions. Using the same brass plates as used with the mica, clamp them together and drill the center hole out to 0.37 cm diameter. Then clamp the grid material between the brass plates one sheet at a time. This will prevent tearing of the material as it is cut to size. Grind the back end of the same drill bit that was used to widen the center hole so that it leaves a sharp edge all the way around. Keep the end of the bit flat so as not to deform the grid material during the cutting. Finally, use the drill bit

as a punch and cut four meshes. More may need to be made for quality assurance purposes. Two meshes should be placed together slightly offset, linearly or at an angle, from one another to make an entry grid with a lower effective transparency. The second grid used on the entry slit was made from a mesh the same thickness as the first but with 59.1 lines per cm so that the transparency is reduced to 91.64%.

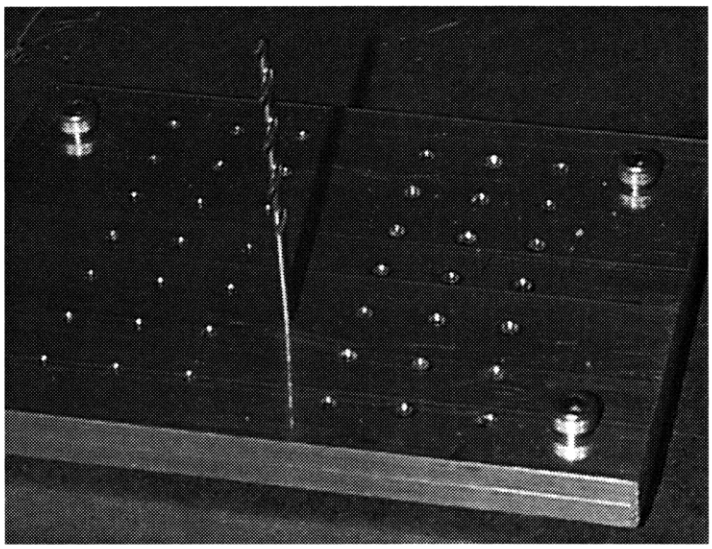

Figure 9. Jig for Punching out Mesh

To connect the grids to the circuit, platinum wire of 0.1 mm diameter was chosen. The wire has high conductivity and deforms easily for sufficient connection to the tungsten mesh as will be seen in the next few steps. Cut a length of wire that can go through about 20-25 cm of the four bore ceramic tubing discussed below. Loop the wire around the same drill bit used to punch out the mesh so that it has just enough material to form a single loop. Next, place the end of the loop and a section of tungsten mesh between two stainless steel blocks and clamp in a vise. This will flatten the platinum wire and press the mesh into the edges providing a semi-permanent bond.

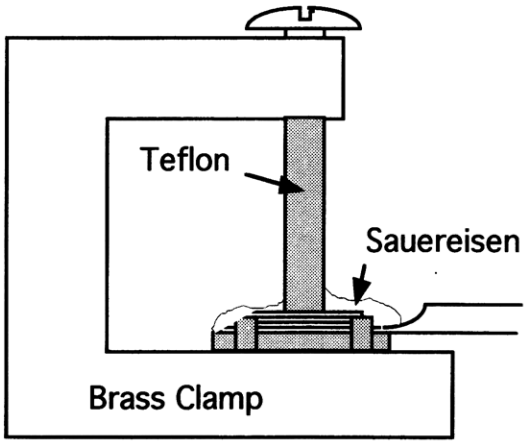

Figure 10. Probe Tip Jig for cementing

Now the individual parts are constructed and the probe head is ready for final assembly.

To house the back of the probe use 5 gauge thin walled stainless steel tubing (ID 5.05 mm, OD 5.56 mm) cut open on one end and flattened to provide a disc shaped paddle of 0.46 cm in diameter. Four bore ceramic tubing is then cut to a desired length for the probe tip, ~25 cm, and placed inside the bore of the tubing. The end of the four bore ceramic should just be even with the "paddle" on the tubing. The four bore ceramic is available from McDanel Refractory or McMaster-Carr and has an outside diameter of 4.8 mm. As for the collector of the probe any conductive material should work nicely, a stainless steel disk was used due to ready availability. Remember to cut one last mica disk of 0.46 cm diameter to insulate the collector from the stainless steel tubing. This disk will not have a center hole.

Build a Teflon/brass or Teflon holder similar to the devices pictured in Figure 10 and Figure 11. Cemented Probe Tip. The Teflon material is used because the Sauereisen cement will not adhere to it during the curing process. Make sure when building the clamping assembly that the central clamp post comes down evenly and

aligned with the aperture of the probe tip. Three or four Teflon posts can be used to position the probe head. Assemble the probe head by first placing the stainless steel tubing on the clamping assembly. Next, place a mica disk without a central hole and then the collector with a platinum loop. Following the exploded diagram (Figure 6) place the components of the probe head down on the clamping mechanism in the correct order. Make sure that the four bore ceramic is included in the assembly. The ceramic should butt against the disk assembly and contain four platinum wires, one in each bore. Turn the central post down until the probe materials are held firmly in place. Carefully place Sauereisen Insa-lute Paste No. 7 around the edges of the probe head. Number seven paste was used due to the increased temperature resistance over the number one paste. In the past, the number one paste has been used on various VTF diagnostics with the understanding that it must be periodically retouched due to the coating flaking off in the high temperature environment.

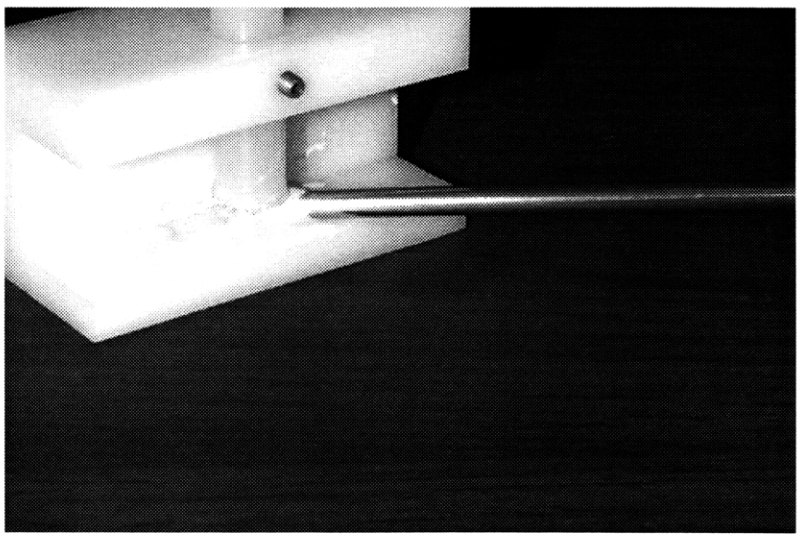

Figure 11. Cemented Probe Tip

Once the cement is dry gently cut the Teflon posts away from the probe and spread paste everywhere as shown in Figure 11. Make sure that the paste extends a little over the end of the four bore ceramic. Once the paste is dry remove the probe from the clamping assembly and coat the backside. The probe tip is complete and now ready to fit into the main assembly.

4.4 Carriage Assembly

The carriage assembly machining is fairly standard on a rotary table equipped milling machine. 2.54 cm thick stock was used to machine the plates based upon material availability in the laboratory but any thickness over 6 mm could be used. The rod stock and bearings were also used from previous experiments and could be substituted with another size.

It is important to note that the machine drawings in **Appendix B. Technical Drawings** are referenced from a center point. For the alignment of the bearings and support rods it is crucial that the plates be machined from a central reference point. The stock can be cut to rough length and then using a center punch mark the midpoint of the plates. When the plates are placed on the milling machine, use a centering bit placed in the punched depression to hold the piece stable while clamping it down. This insures that the carriage will slide freely on the rails when the assembly is complete. Also of note with this system is the fact that the outside dimensions of the plates are not critical to the operation of the device. Therefore, great care is not needed when finishing off the rough cuts. Figure 12 through Figure 18 show various stages of machining up to the finished plates.

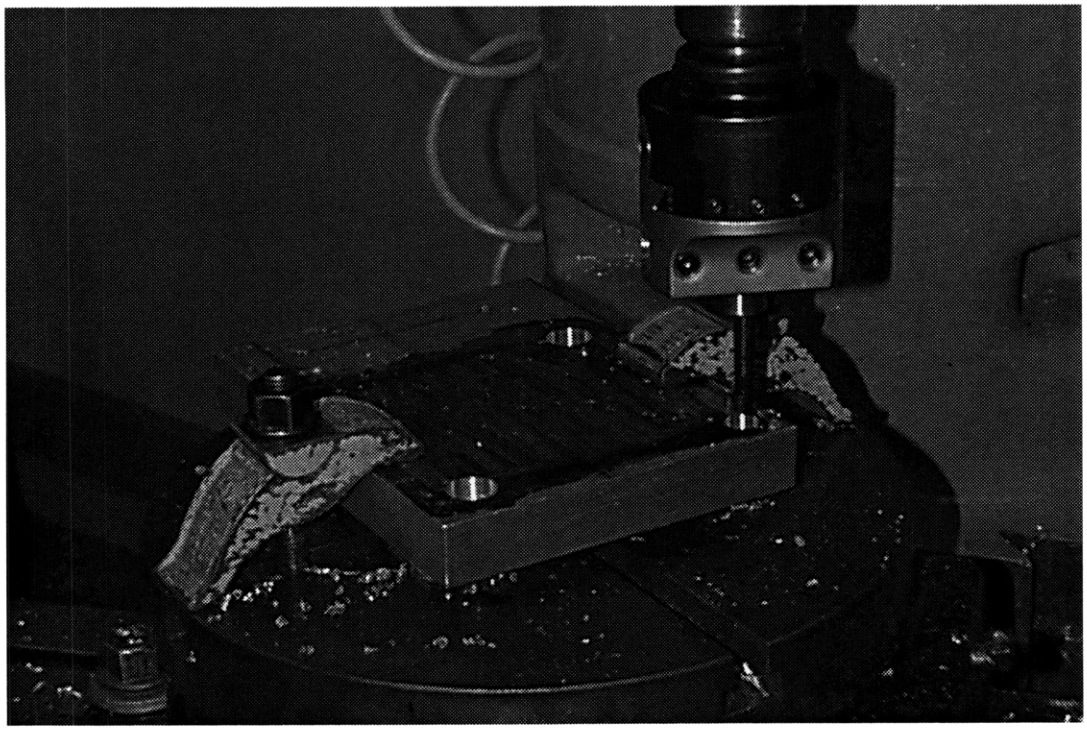

Figure 12. Support Plate on Milling Machine

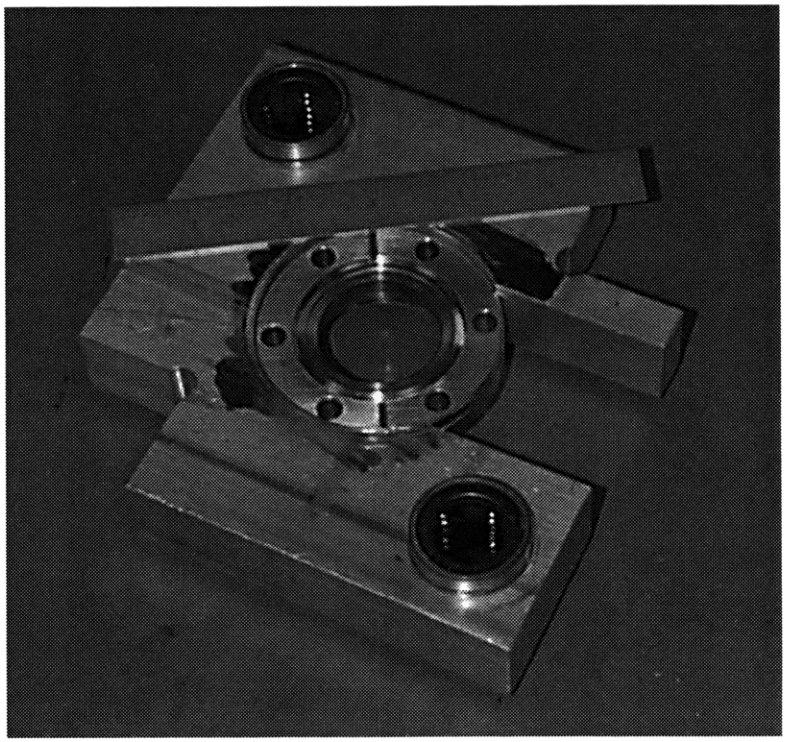

Figure 13. Machining a Carriage Plate

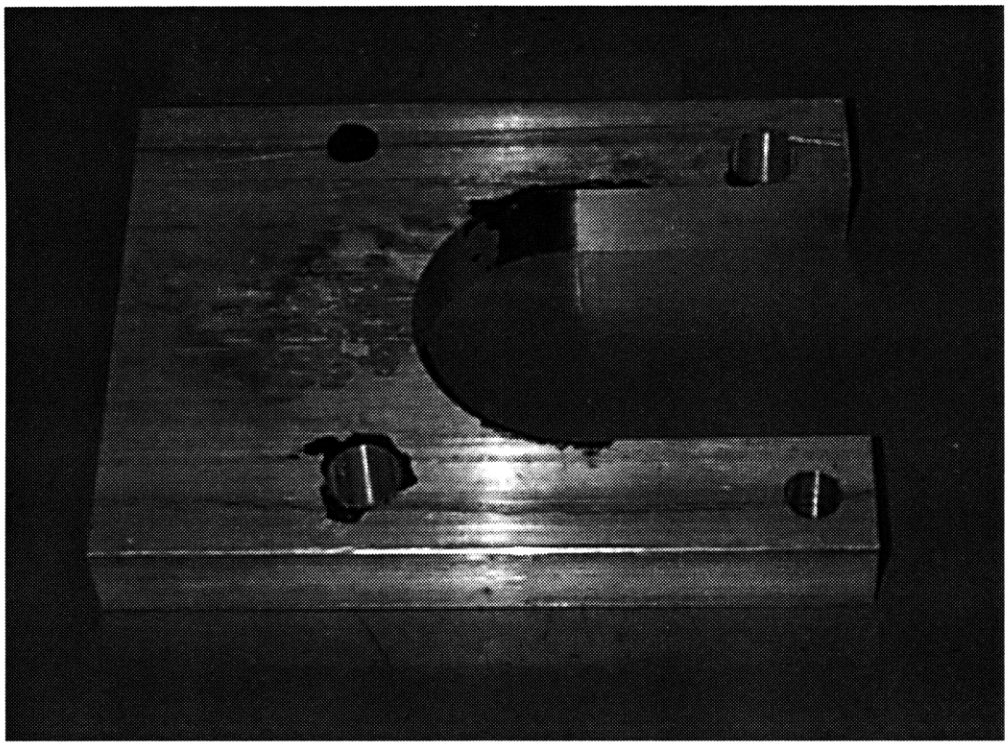

Figure 14. Making the Support Plate

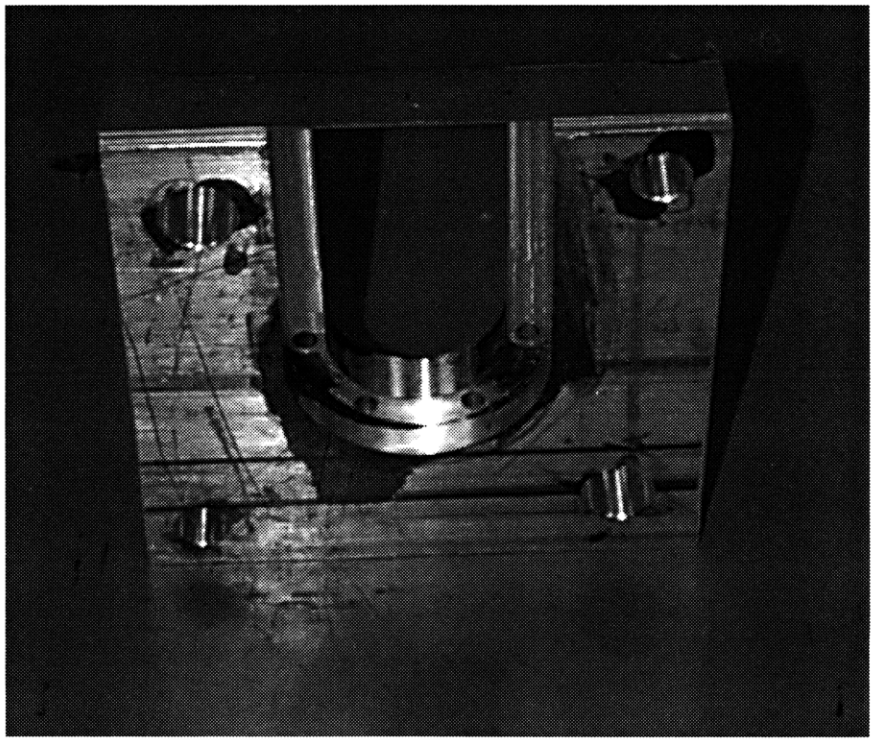

Figure 15. Machining the Mounting Plate

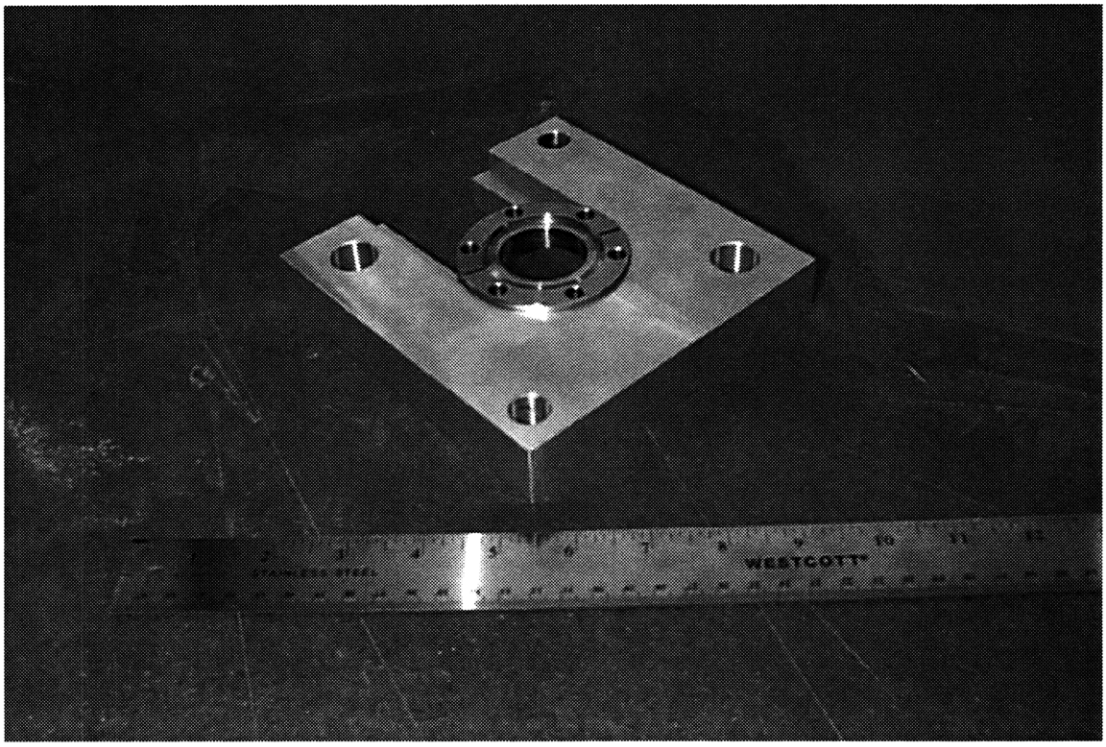

Figure 16. Mounting Plate

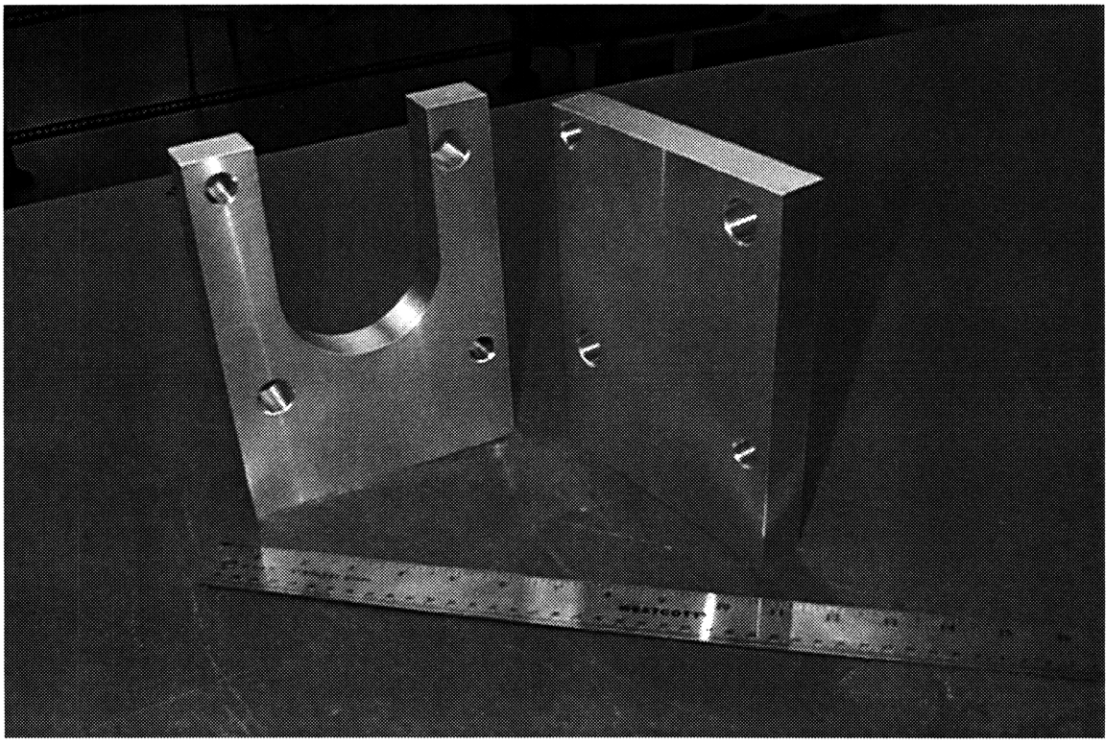

Figure 17. Finished Support and Back Plate

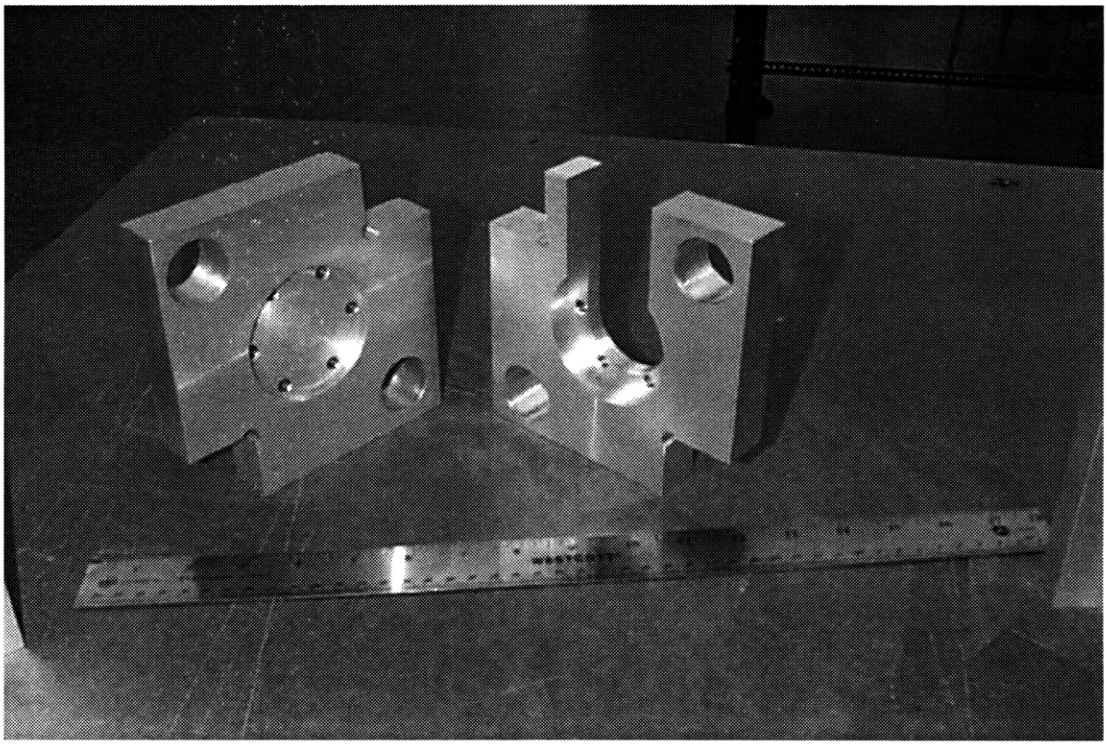

Figure 18. Finished Carriage Plates

The probe carriage is made of standard stainless steel vacuum hardware with a welded bellows to allow for radial movement. A stainless steel tube press fit into a Teflon bushing in the carriage fits within the bore of the bellows and extends 1 m. The tube provides structural support and houses the leads from the probe tip. The probe tip is fastened to the tube by the use of a set screw. This insures that the tip does not move radially without the carriage and maintains oriented with the toroidal magnetic field lines.

4.5 Electrical System

The signals are carried from the probe tip by electrical wire interior to the tubing connected to an electrical feedthrough on the carriage. Extreme caution must be used when handling the platinum wire at the end of the four bore ceramic since it

has a tendency to break on the edge. Sauereisen paste was used to insulate the bare wires from each other and provide protection from the edge of the four bore ceramic. Insulated connectors were soldered onto the platinum leads exiting the four bore. Connectors were also placed on the wires that run the length of the stainless steel tubing. This enables quick and easy replacement of probe tips. Table 4 and Figure 19 contain wiring colors and pinouts for use in maintenance and debugging.

Connection	Wire Color
Electron repeller or entrance grid	Green
Ion repeller or sweep grid	Blue
Electron suppressor or secondary emissions repeller grid	Yellow
Ion Collector	Red

Table 4. Wiring Information

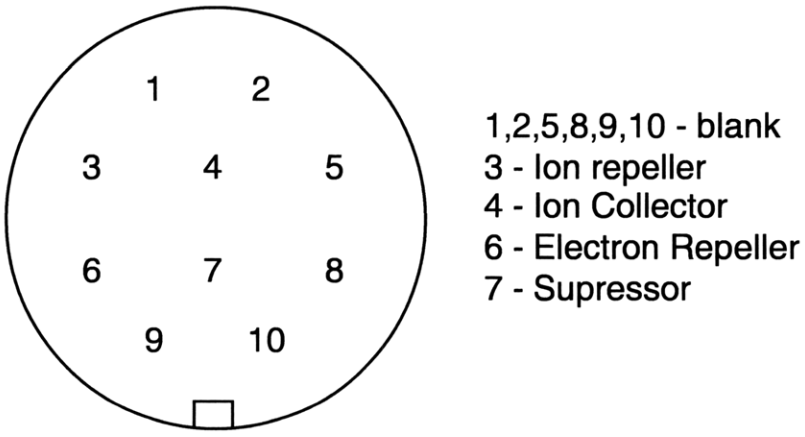

Figure 19. Pinout Diagram

A simplified diagram of the electrical system is contained in Figure 20. A software based digital low pass filter is used to reduce RF signal noise that reaches the probe electronics. The noise is primarily caused by the rectification of the 2.54 GHz RF into its 180 Hz power envelope.

The probe bias , V_b, is provided by a KEPCO BOP-500 amplifier. The amplifier inputs can be driven by a function generator or by the method detailed in **Section 4.6 Computer Interface**. The sense resistor produces a voltage proportional to the probe current. The resistor value is chosen to be large enough to provide a large signal compared to ambient noise but small compared to the probe bias.

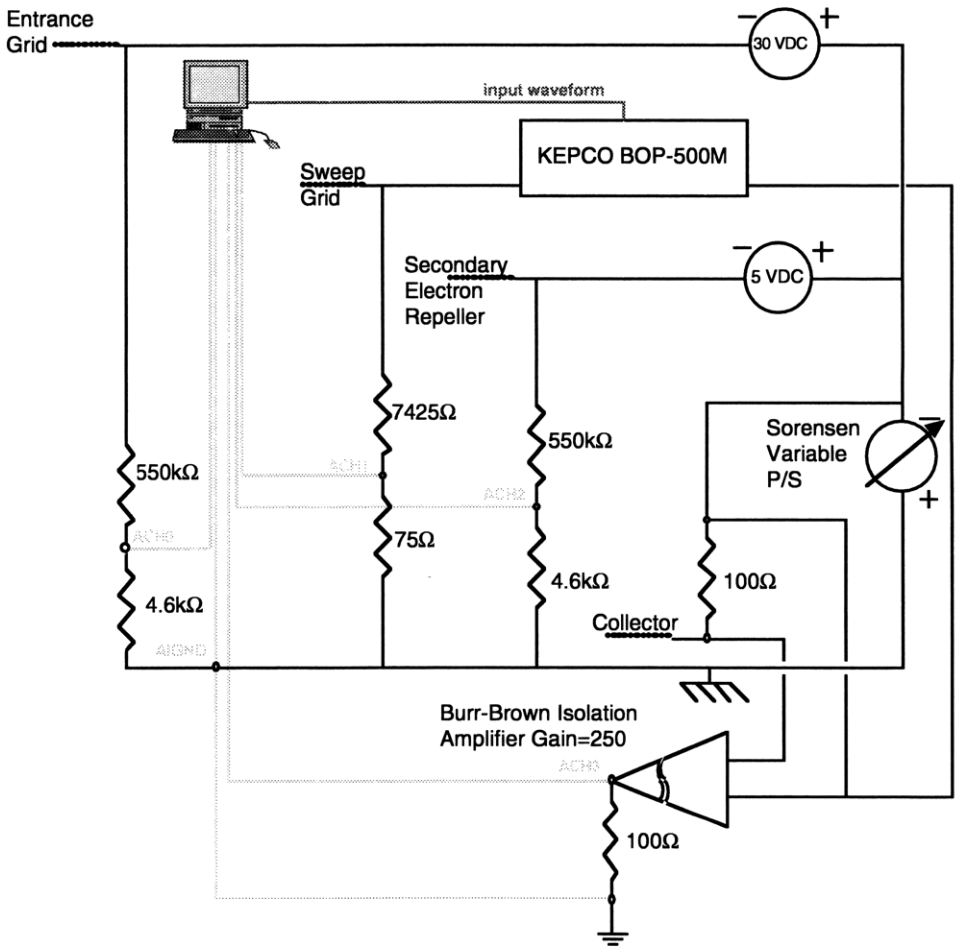

Figure 20. Electrical Schematic

4.6 Computer Interface

As discussed in Section 2.5 VTF diagnostics interface with the PC in the control room through the CAMAC crate via a GPIB interface. VTF is currently in the process

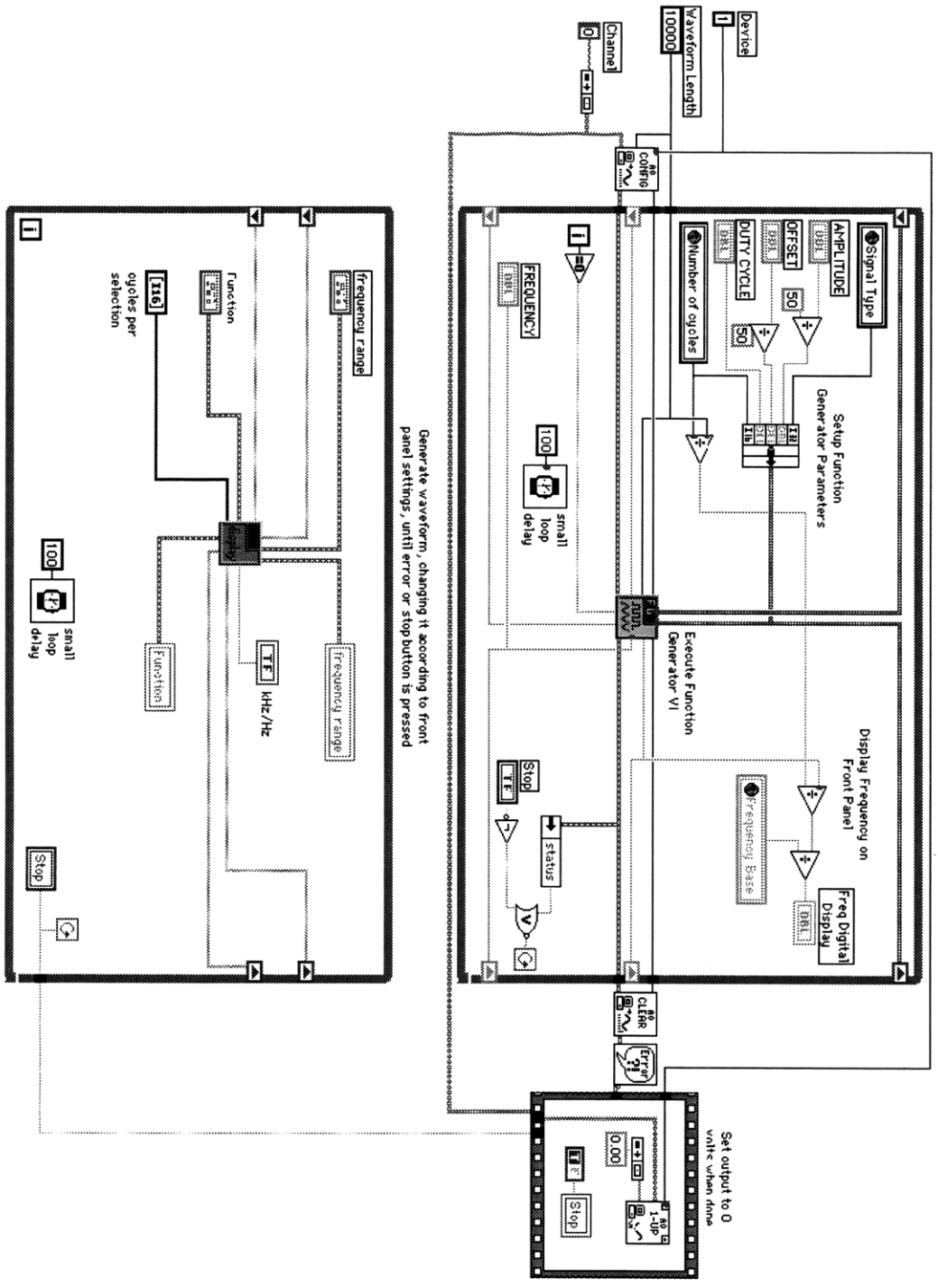

Figure 21. LabView Function Generator VI

of updating the data capturing system into a LabView environment. The GEA is the first diagnostic to use the new LabView interface. A Packard Bell R5215 Pentium 200

using a NIDAQ PCI-1200 data acquisition card outputs a waveform programmed by the operator to the KEPCO BOP-500 programmable power supply. The same PC is used to receive the signal from the collector circuitry described in Section 4.5.

LabView uses a graphical programming language so the program routines are quite easy to interpret. The first program shown in Figure 21 is responsible for generating and outputting a waveform to the KEPCO BOP-500M. This program takes input from the virtual knobs and indicators on the computer screen and uses that input to calculate the waveform shape and then "writes" the result to DAC0OUT channel of the NIDAQ PCI-1200 card. This waveform is then amplified by the KEPCO BOP-500M into the desired sweep waveform.

The second program (see Figure 22) is responsible for capturing the data and archiving it to the computer hard disk. The program first looks at the type of data acquisition mode the user would like to use. Using a simple case statement the program then either executes the manual acquisition code or the automatic mode.

If the user selects the manual acquisition then the computer begins to sample the first four analog input channels on the NIDAQ PCI-1200. The samples are captured and then the values are scaled back to a value representative of the grid bias voltage. The values are then appended to the end of a tab delimited text file specified by the path name in the program. The data is saved as a scaled value corresponding to the actual grid voltage not as a sampled voltage between -5 and 5 volts. The collector data is stored as a current value in microamperes. This method of data capture is not a buffered input and therefore the rate of capture is completely dependent on the speed of the computer and the task load of the processor. Data

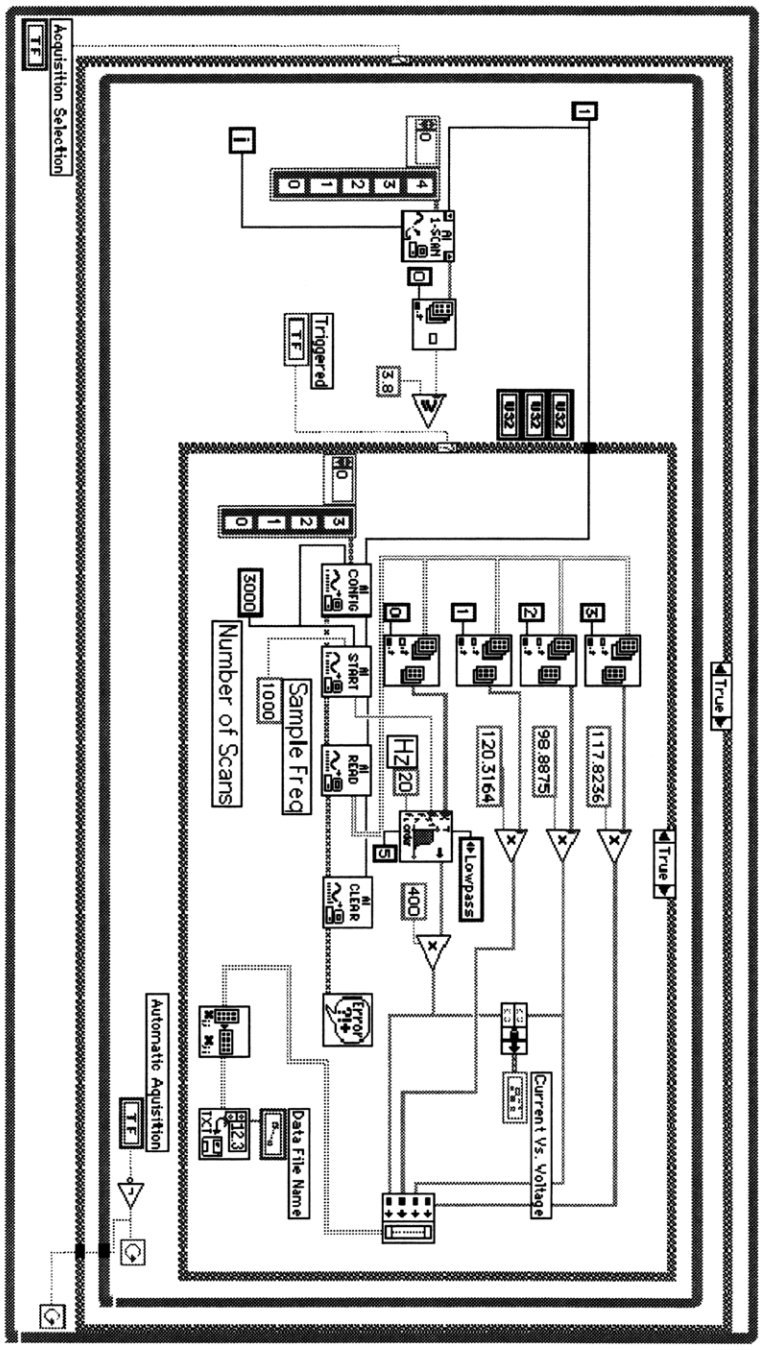

Figure 22. GEA Main LabView VI

capture rates are quite frequently between 200 to 400 samples per second on each channel. This is not the preferred method for capturing experimental data. The purpose of this function is to allow the user to view the biasing voltages on the grids

to ensure proper operation and to give a quick view method for troubleshooting any problems that may occur. Data capture starts immediately after executing the program and does not stop until the user cancels the operation.

The automatic acquisition mode case of the loop is more complex. When the program starts execution channels are sampled as in the manual case. Each sample of ACH4, the CAMAC trigger, is compared to see if it exceeds 3.8 volts. If the threshold is not exceeded the program simply does nothing as seen in Figure 24. If the threshold is exceeded the actual data sampling occurs as shown in Figure 22. The triggered light on the users control panel is set to on and the first four channels are sampled. A buffered sampling occurs in which the samples are stored in the computer memory until all three seconds of data have been taken. The computer's clock controls the data capture rate, which is set at 1000 samples per second. This sampling rate is then fed into the processing section of the program to allow digital filtering to occur. After all 3000 samples per channel have been taken the program then proceeds to process the data. Data processing scales the input value back to a value that corresponds with the grid voltage prior to using the voltage dividers shown in Figure 20. In addition, the high frequency noise generated by the electron beam emitter power supplies is also filtered out by adding in a digital low pass filter. A fifth order software Butterworth filter is used with a pass frequency of 20 Hz. In the early testing stages before this filter was added the probe traces were frequently obscured by the noise. After filtering the data is then returned into a two dimensional array and written to a tab delimited text file specified by the user. The values are recorded as voltages with the exception of the collector, which is saved as current in

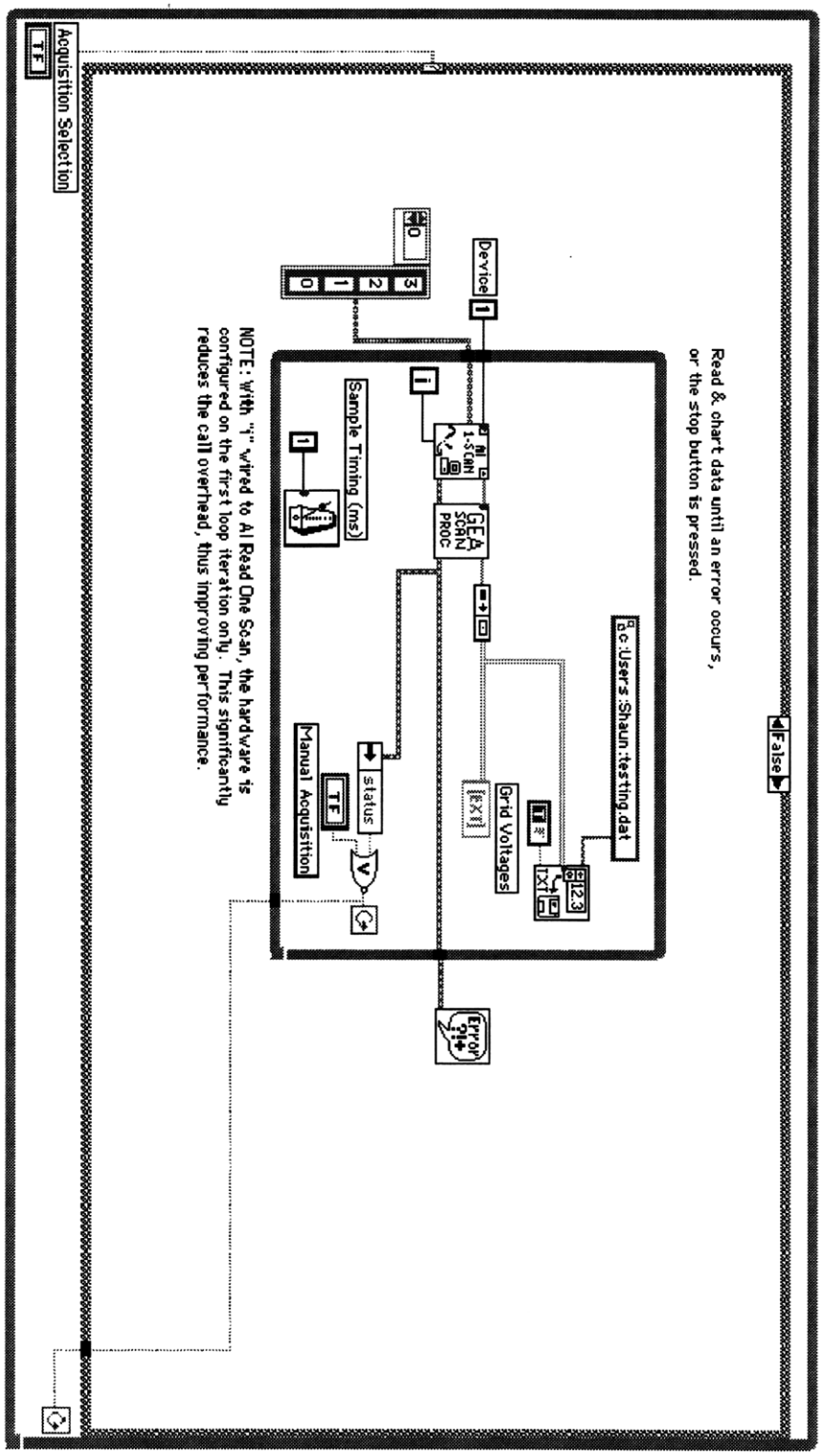

Figure 23. GEA LabView VI Manual Loop

microamperes. Simultaneously, the output is directed to the screen where the user can see a current versus voltage probe characteristic. This allows the user to make a rapid determination on the quality of data received. In addition, parameters can then be changed immediately for the next plasma shot allowing for better data collection. The program then exits the case loop and samples data looking for ACH4 to exceed the threshold value again. This process continues until the user selects cancel and halts the automatic acquisition.

Other modules can be written and added or removed as necessary to provide the operator with the most efficient method for viewing data collected from the GEA.

Eventually, it is the hope of the author that the Paragon interface and the LabWindows environment running on two separate PCs will be replaced by LabView executing on one PC with a second PC as a backup.

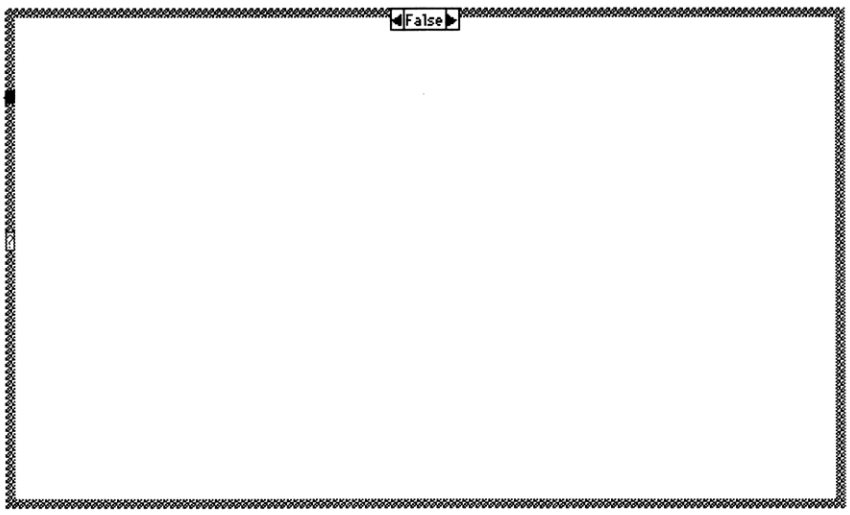

Figure 24. GEA LabView Not Triggered Loop

4.7 Operation

The operation of the GEA is fairly simple when compared to the complexity of the VTF device itself. After the VTF is set up to run plasma shots the GEA must be powered on in the cell. Control of the equipment can be done remotely from the control room. Adjust the position of the probe tip by loosening the clamps and sliding the carriage assembly so that the desired radius is achieved, see Figure 25. There are three power supplies that must be powered on and adjusted for performance. All three are located on the GEA stand (Figure 26).

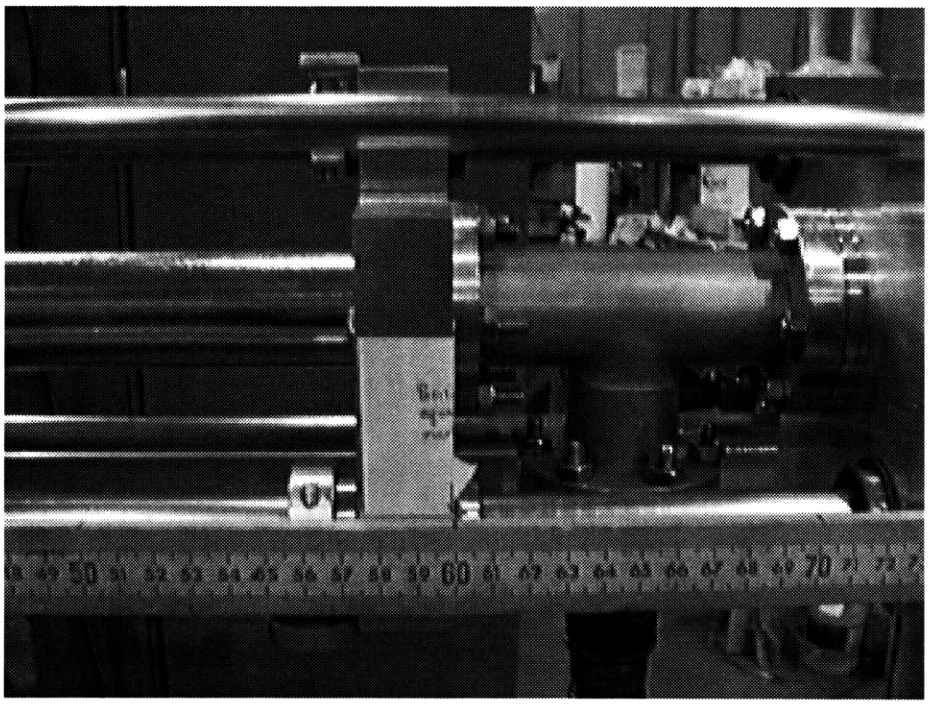

Figure 25. GEA Position Indication

The first supply is the KEPCO BOP-500M. Check that the mode selector switch is in voltage mode. Check that the bipolar voltage control switch (upper left corner as facing the front panel) is in the on position. Next the main power switch must be placed in the on position and the supply must warm up for three minutes. After the

warm up period is over check to make sure the power supply is working by examining the output light with a lightning bolt painted on the face is lit. Another light in the center of the left amplifier icon should also be lit showing that the supply is in voltage mode.

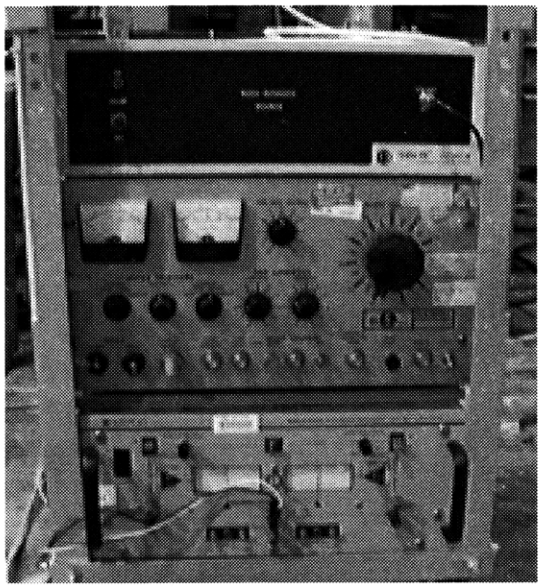

Figure 26. GEA Stand

The second supply is the GEA main circuit. This box houses the 5 volt and 30 volt power supplies and the isolation amplifier and associated circuitry. Simply flip the power switch on the left hand side to the power position. Verify the power is on by examining the power light on and the cooling fan in operation.

The final supply to power up before closing out the VTF cell is the Sorensen High Voltage power supply. Use caution when operating this supply since it is capable of generating 2000 volts. First check that the voltage adjust knob is turned completely counter clockwise. The power supply has an interlock which will not allow power to come on if the knob is not placed in the zero position. Next, turn on

the main power switch in the lower right hand corner of the front panel. The red reset button must then be pressed momentarily and then the high voltage button can be depressed. Finally adjust the voltage adjust knob until the desired voltage is reached. The voltage should be set to a value on the meter, which is approximately 10 volts above the plasma potential at the probe tip position. This sets the entrance grid to a voltage approximately three to four times the electron temperature plus the plasma potential. The meter shows the voltage to which the collector is biased. This value will be 30 volts more positive then the entrance grid. For example, if the Sorensen high voltage supply is adjusted to the meter reading 250 volts the entrance grid is biased to –280 volts, the secondary repeller is biased to –255 volts, and the collector is set at –250 volts.

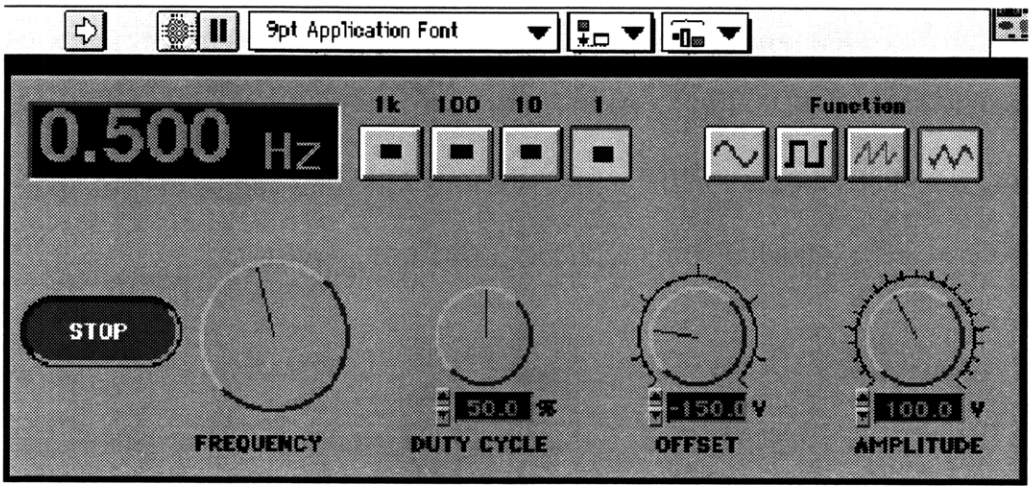

Figure 27. GEA Function Generator User Interface

When changing the probe position in between plasma shots be careful to change the bias voltage accordingly to avoid overheating the grids by drawing a large current. The grids do not actually melt but experience shows they can deform and

make electrical contact with other grids. This obviously results in replacing the probe tip.

Controlling the programmable power supply and therefore the sweep grid voltage is done by using the LabView environment on the Packard Bell R5215 PC located in the control room.

Before starting plasma shots start the LabView program by double clicking on the icon. LabView will then ask for several options. Choose the **Open VI** option. When the dialog box asking for the VI (virtual instrument) comes up change to the **User.lib** directory and choose the **GEA Function Generator**. A window should open with controls as shown in Figure 27. This VI is used to control the waveform output to the sweep grid. Select the operating tool (it looks like a hand) in the tools palette as shown in Figure 28. The controls can be changed by clicking in the numerical boxes and entering changes by typing the desired values or by pushing the buttons and turning the knobs located on the panel. Various functions can be output and frequency can be adjusted along with DC offset and amplitude.

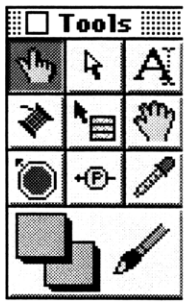

Figure 28. LabView Tools Palette

Next select **File...Open...** and select **GEA Chart**. There will now be a second window as shown in Figure 29. Ignore this window for now. To actually start the

function generator executing the run arrow in the upper left corner of the GEA Function Generator window must be depressed. To stop the VI execution depress the stop button.

With the function generator running switch back to the GEA Chart window. This is the VI created by the second program described in **Section 4.6 Computer Interface**. From this window the data will be collected, processed, and written to a file. There are two options available for this VI. The first is a manual data collection scheme that can be used for troubleshooting and to examine proper grid biasing before introducing a plasma. The second mode is the automatic data capturing mode which is much faster and should be used for actually gathering experimental data.

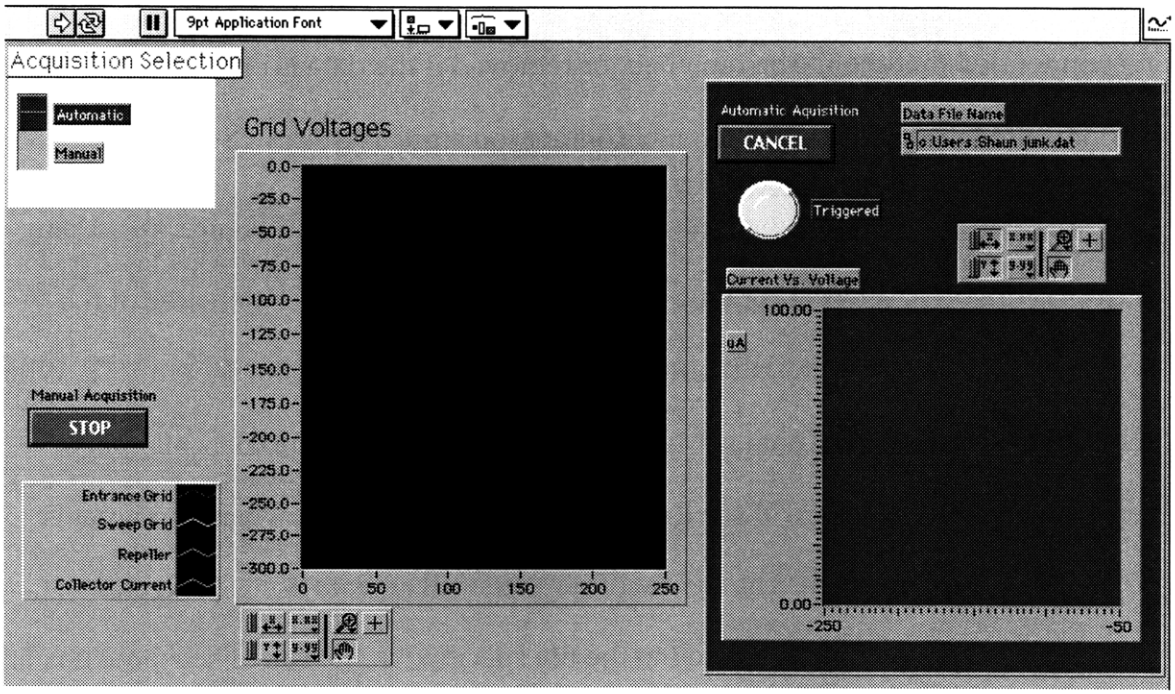

Figure 29. GEA Chart VI

To operate the GEA in manual mode position the Acquisition Selection slide switch to manual using the operating tool. Depress the run button with the operating

tool and data collection will commence. The graph will start recording data immediately in a strip chart format. Thus, the horizontal axis is time steps, which are referred to in the LabView documentation as NIDAQ points. The graphical output is the actual grid voltages for each of the grids. The collector data is output in microamperes. To change how the data is viewed controls are located below the chart. The user can zoom in or out on specific data and see the values for specific points. See the LabView documentation for more specific instructions on the graph tools. When the user would like to stop data collection depress the manual acquisition stop button with a click of the mouse. The data is recorded to a file in a path specified in the LabView program (see **Appendix C. LabView Program**). The data in this mode is appended to the file each time it is run. Therefore, it is recommended that the file be renamed, or removed if the data is of no use, periodically to prevent the file from becoming too large to work with.

The second mode of operation is the automatic mode (see Figure 30). Using the operating tool, select automatic mode in the Acquisition Selection area of the window. Next, depress the run button and then conduct a plasma shot in VTF. When the CAMAC engineering data is triggered the computer will automatically begin recording data. The user will see the triggered light turn green when the signal is received by the computer. The light will stay on until all data is collected and processed. Then the data is written to the file specified in the Data File Name box and a probe characteristic curve is output to the screen. The graph shows probe current in microamperes versus sweep voltage in volts. The probe current versus sweep voltage data can then be further examined using the graph tools located above the graph. The

computer will continue looking for a CAMAC trigger and repeat the process. The user can stop the computer by pressing the cancel button at any time.

To change the data file name from shot to shot the user must depress the cancel button and then change the file name. To start automatic acquisition again the run

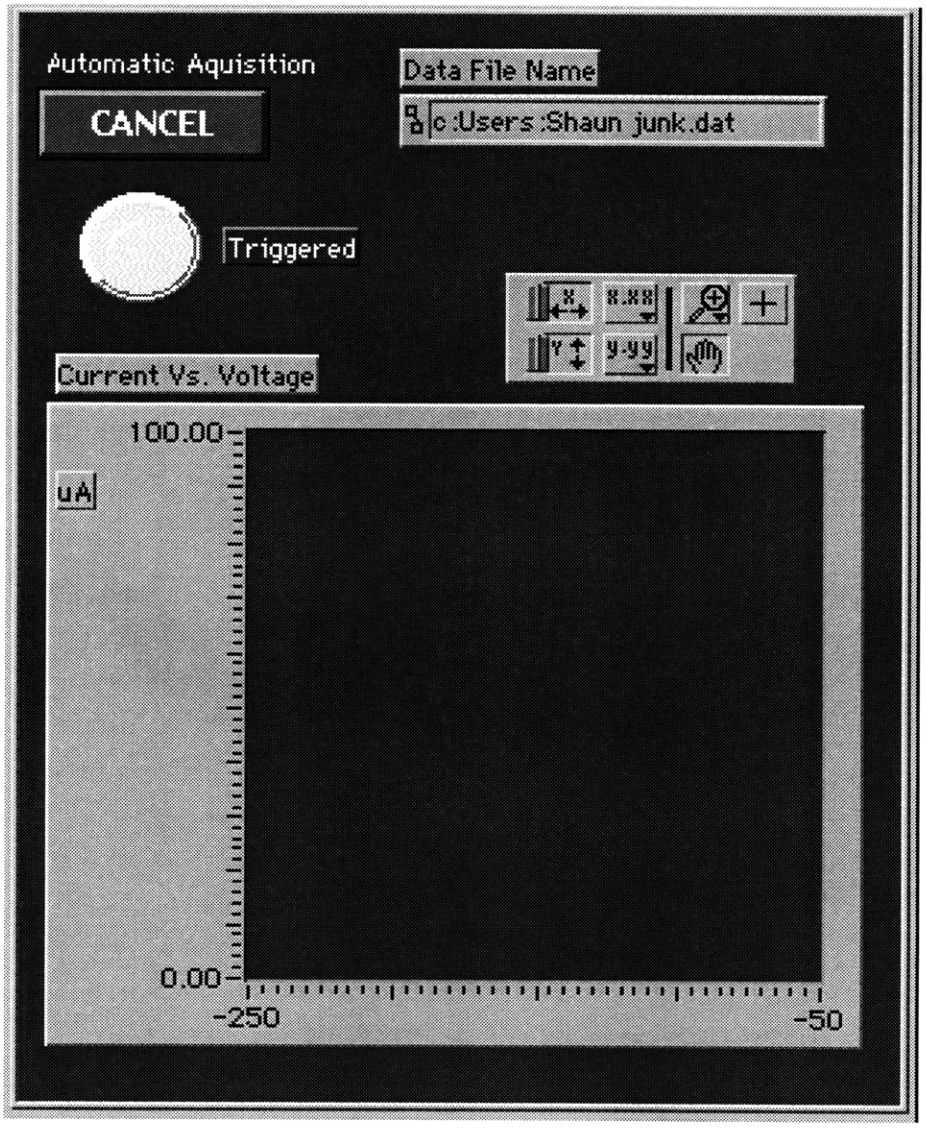

Figure 30. GEA Chart Automatic Acquisition

button must be depressed. It is important to note that the data file is not appended in this mode. Instead, the user must change the file name each plasma shot unless the

user desires to overwrite the data from a previous shot. The program will display a dialog to confirm that the user wants to overwrite the file, if not, the user can click on a cancel option to avoid overwriting an existing file.

5. Measurements

5.1 Procedure

The first probe assembly was completed on January 3, 1998. Once the probe was constructed several plasma shots were run to verify proper operation. The debugging stage went through two probe tips before operation was determined to be at a satisfactory level. The first tip was lost due to an electron beam plasma arcing to the probe which was placed in a radial position directly above an emitter. Figure 31 shows the remains of the first probe tip.

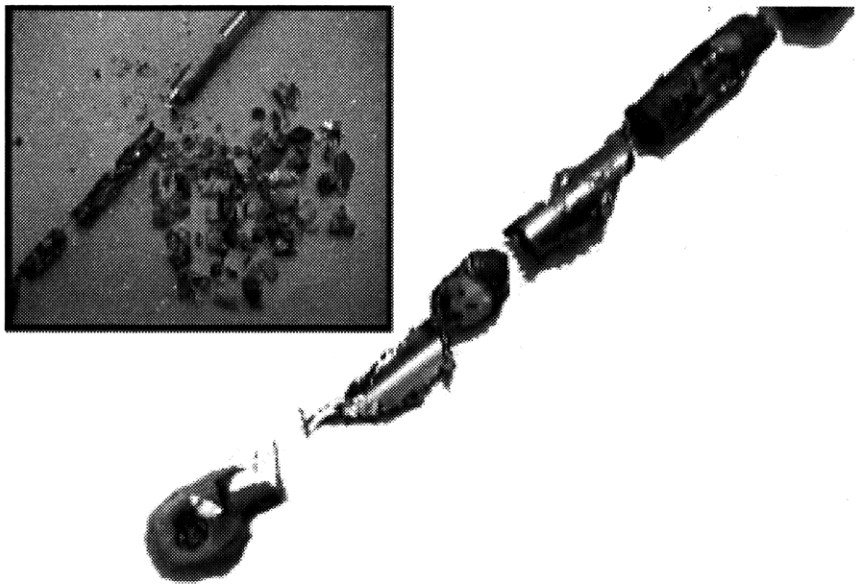

Figure 31. Probe Tip Damaged by Plasma Arcing

Occasionally, the plasma beam has arced to the chamber wall due to various causes such as power supply failure or insufficient chamber conditioning. To minimize the probability of another GEA being destroyed the probe was moved to a port located away from an emitter. The second tip was melted due to a mistake in connecting power supplies by the author. This was corrected and the wires for the supplies are color coded to match their post connections. The data presented in this section was taken during March 9-13, 1998 with the second probe tip before the entrance grid was destroyed. Currently, a third probe tip is mounted in the VTF but it is unable to produce useful data. The problem is believed to be a electrical connection near the tip. The current tip has not operated correctly since installation. Examining the circuit reveals correct operation from the electronic circuitry to the computer. Therefore, the problem is believed to be located in the cemented region of the probe tip where voltage cannot be examined. The cause of the problem is most probably a break in the platinum wire leading to a grid. This open circuit would not be measured in the voltage sampling. Materials to build another tip are on order but were not available to make another tip for testing at the time of this writing.

The probe is mounted at a port between magnets 190 and 200. Unlike most of the diagnostics on VTF, which are mounted at the mid-plane, it is mounted two inches below the mid-plane. This arrangement is due solely to the availability of ports. Shots were taken between a major radius, R, of 108 cm to 117 cm. At this range of positions the floating potential of a plasma beam shot was approximately -200 volts.

Electron beam plasmas were generated with two filaments and a toroidal field current of approximately 5000 A. Beam current for each shot was consistent at approximately 100 A.

Several plasma shots were run without observing a useful probe characteristic.

To verify proper operation, the probe was run in a Langmuir probe mode. This gave the ability to check its results with previous data (Moriarty, 1996). Ten shots were run in this mode. Five shots were taken at R=117 cm and five were taken at R=110 cm. The entrance grid was swept with the KEPCO BOP-500M and the voltage was determined from the sense resistor, which was set at 10 Ω. Figure 32 shows a

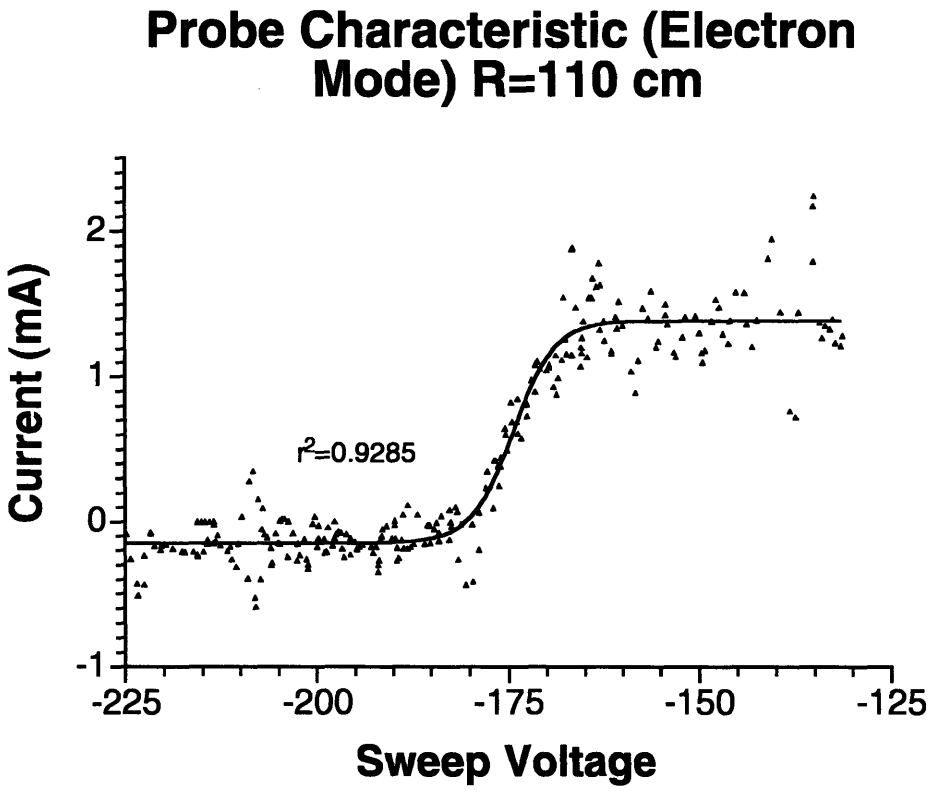

Figure 32. Typical Probe Characteristic (Langmuir Mode)

probe characteristic trace. These traces were then differentiated to find a distribution function. Figure 33 and Figure 34 show typical distribution functions. It is important to note the tail in Figure 34. This tail of extremely energetic electrons were important when trying to operate the GEA in ion detection mode.

Initially, a smaller Sorensen power supply was used since it was assumed that floating potential was not quite as negative and it was not expected to have a tail of highly energetic electrons present. Since the probe is mounted further below the mid-plane the floating potential was significantly more negative than readings from previous probe mounted at the mid-plane predicted. In addition, it proved necessary to bias the entry grid to approximately -365 V in order to stop electrons from entering into the probe chamber.

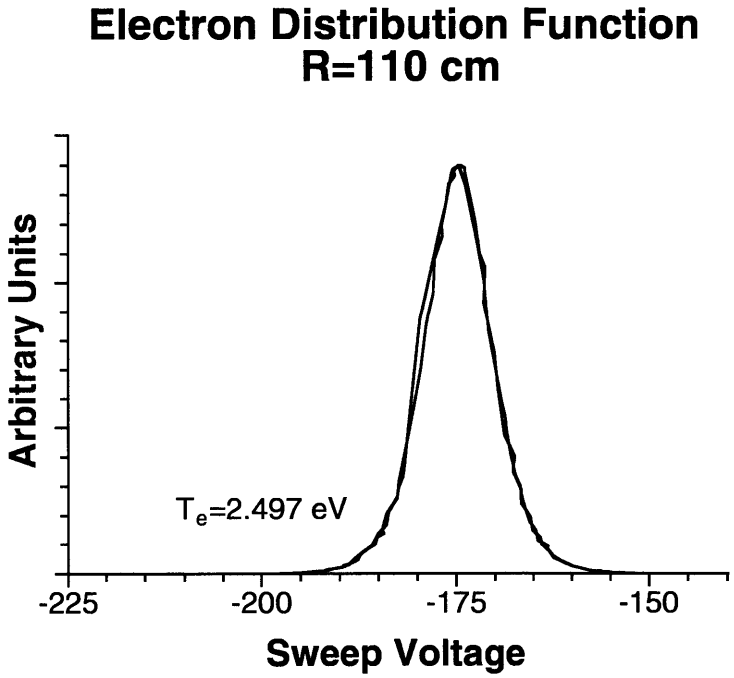

Figure 33. Electron Distribution, R=110 cm

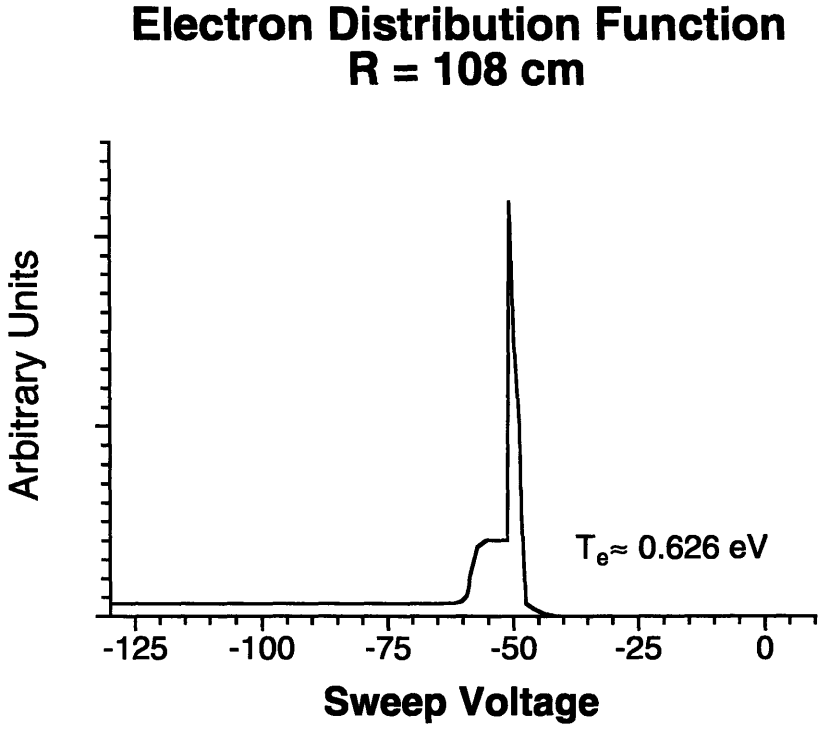

Figure 34. Electron Distribution, R=117 cm

The bulk temperatures of the electron species agreed well with prior electron temperatures determined by Langmuir probe traces, always within 22%.

5.2 Ion Energy Distribution

Once the probe had exhibited the ability to read electron information the circuitry described in **Section 4.5 Electrical System** was attached and plasmas discharges were conducted with the probe set to collect data. Forty-three electron beam plasmas were diagnosed at various radii between 108 cm and 117 cm. Typical data can be found in Figure 35 through Figure 42. Distributions proved to be Maxwellian with a high degree of fit (r^2 values in the .85 to .95 range). The data scatter is imposed due to interference in the circuitry from various power supplies. After this data was collected a digital filter was added in the LabView acquisition program.

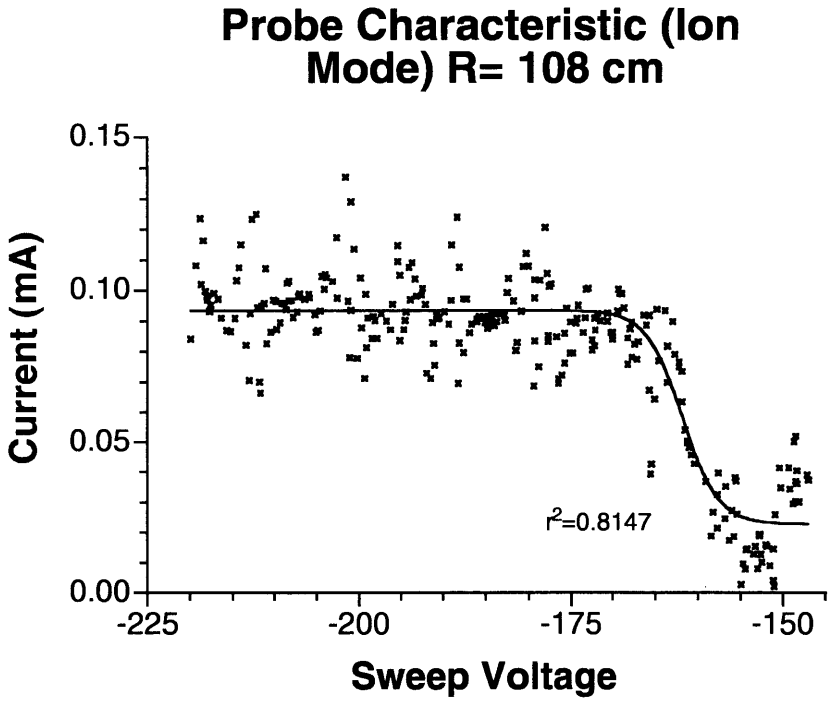

Figure 35. Probe Characteristic, R=108 cm

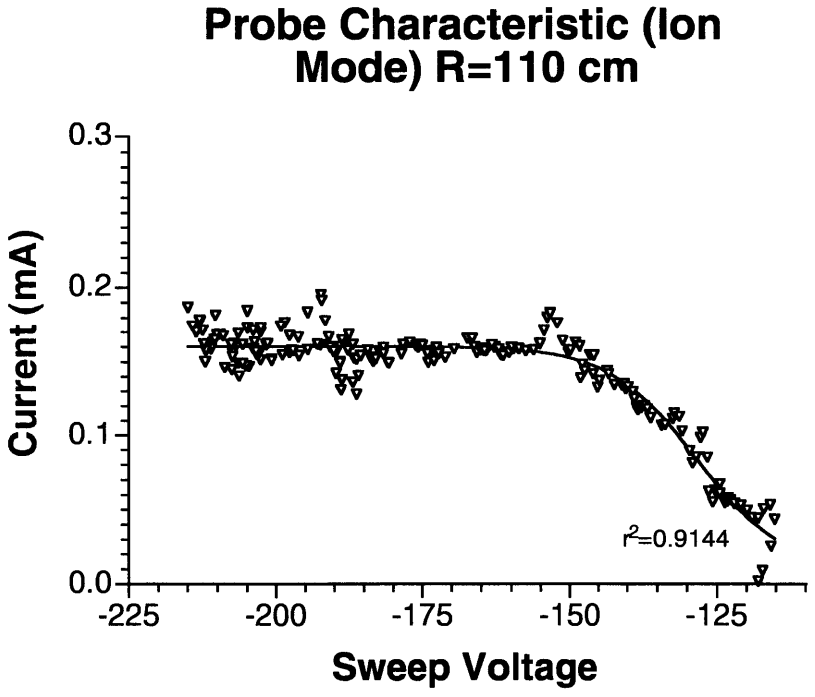

Figure 36. Probe Characteristic, R=110 cm

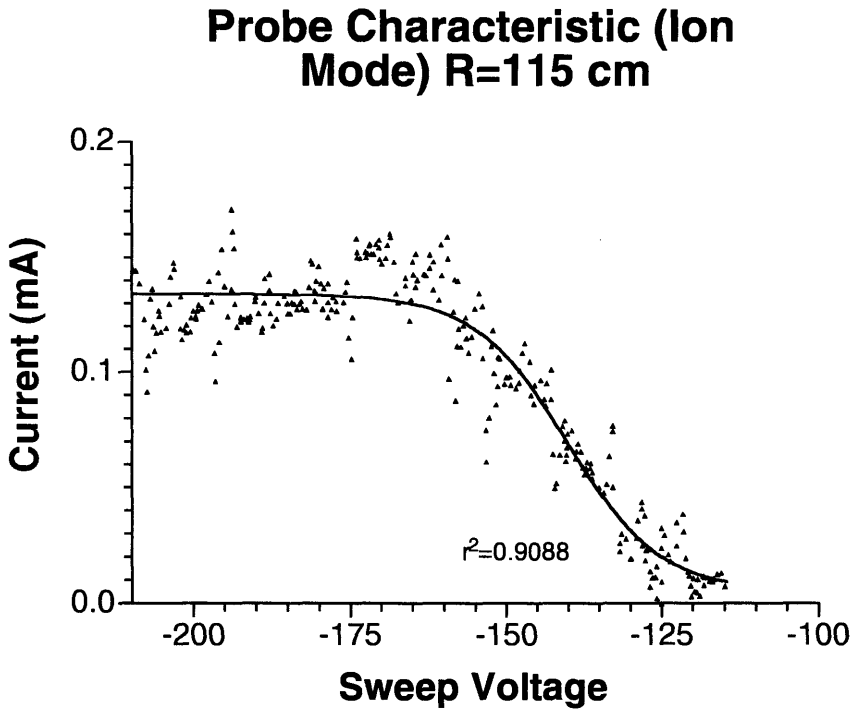

Figure 37. Probe Characteristic, R=115 cm

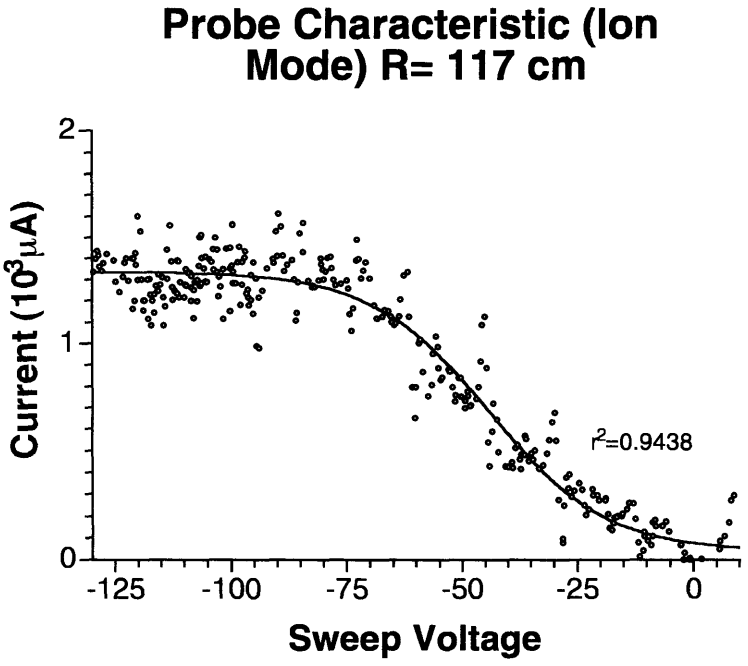

Figure 38. Probe Characteristic, R=117 cm

5.3 Ion Temperature Measurements

The surprising results were that of parallel ion temperature, $T_{i_{\parallel}}$. As can be seen from Figure 39 through Figure 42 the temperature was much higher than expected. Although I have only included four graphs, which vary widely in temperature, $T_{i_{\parallel}}$ was fairly consistent with radius. Typical data revealed $T_{i_{\parallel}}$ to be uniformly distributed across the radii examined at about 8.5 to 8.6 eV. However, more data is needed to be conclusive. Temperature varied widely from one shot to the next and, as can be seen from the data presented, results were obtained anywhere from 2 eV up to 13.6 eV.

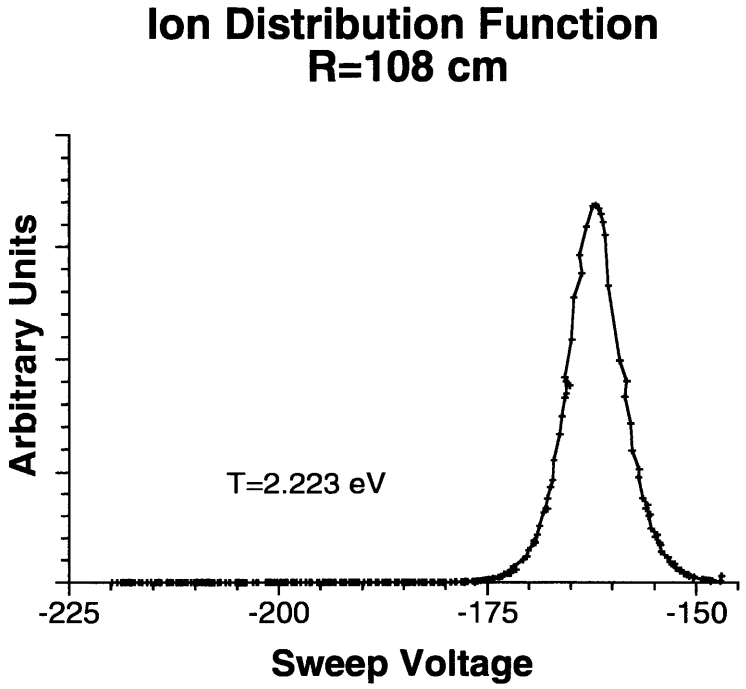

Figure 39. Ion Distribution, R= 108 cm

This data suggests that ion heating processes are more prevalent than VTF researchers previously thought. This has been observed in laboratory electron beam

plasmas before (Wong et al., 1964; Beiersdorfer et al., 1995; Kolyada et al., 1977). In the VTF case, a plausible explanation seems to be the Landau Damping of the ion acoustic wave.

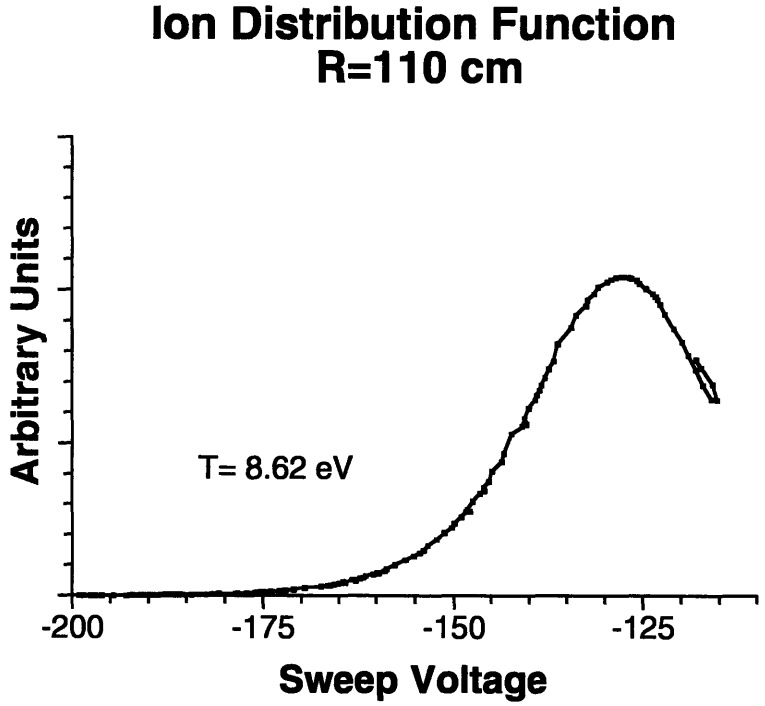

Figure 40. Ion Distribution, R=110 cm

Ion acoustic waves are low –frequency longitudinal plasma density oscillations in which the ions and electrons move in phase. These waves differ from conventional sound waves in that the coupling between electrons and ions arises from their electric fields. A number of authors (Nicholson, 1983; Krall and Trivelpiece, 1973; Gould, 1964) have shown that the ion waves can exist in plasmas even without collisions. These equations even predict strong damping by interactions with ions moving at velocities close to the phase velocity of the wave.

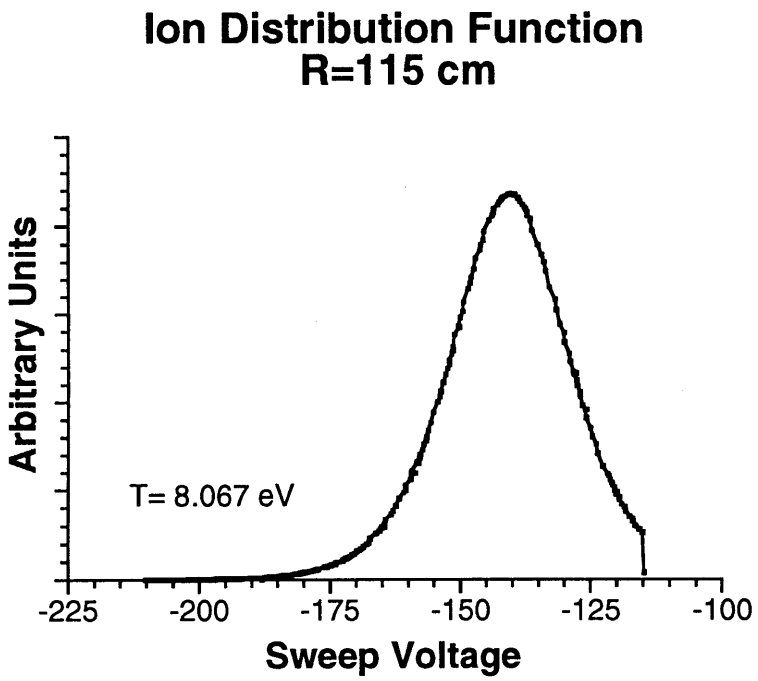

Figure 41. Ion Distribution, R=115 cm

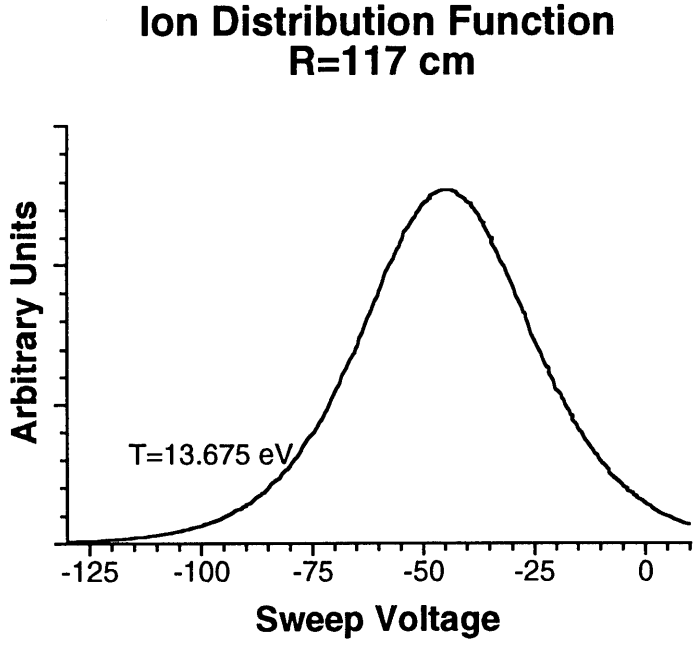

Figure 42. Ion Distribution, R=117 cm

The VTF results are consistent with those of authors mentioned above (Wong et al., 1964; Beiersdorfer et al., 1995; Kolyada et al., 1977) in the fact that they observed electron beam plasmas with T_e comparable to T_i. Some researchers (Yajima, et al., 1978; Kaya, 1982) were even able to observe the ion acoustic wave contributing significantly to the heating of ions due to the drift velocity of the ions matching closely with the wave velocity. In addition, prior experiments have revealed the suspected presence of the ion acoustic waves in the VTF machine (Moriarty, 1996; Riddolls, 1996). By combining the emission spectra with velocity distributions obtained with the GEA a strong theoretical analysis could be made incorporating quasilinear diffusion theory and strong turbulence. A study along these lines might liberate the source mechanism for ion heating.

6. Conclusion

6.1 Summary

VTF was constructed to simulate an ionospheric plasma environment and to cross check laboratory experiments with data taken at Arecibo, Puerto Rico. Many different diagnostic devices has been installed and removed from the experiment since its beginning in 1990.

This paper provides the practical knowledge and theoretical guidance necessary for the proper construction of a gridded energy analyzer for the Versatile Toroidal Facility.

First, background information was given about the Versatile Toroidal Facility. VTF was constructed to provide a laboratory environment in which data from

Arecibo, Puerto Rico could be correlated to a more controlled environment. Accurate and reliable diagnostics are needed to provide the necessary laboratory data for cross checking. The operating conditions of the VTF were instrumental in designing a gridded energy analyzer that would function reliably and accurately.

In Section 3, a theoretical background was determined for the design of the GEA. A discussion of Langmuir probe theory developed the understanding necessary to apply the results to the application of a GEA. We saw that in order to avoid the space-charge limitation the grid spacing could not exceed 0.4 mm. A simple GEA design was discussed and a slightly more complicated design was chosen for better performance. A secondary emission electron repeller grid was added in front of the collector plate to reduce errors caused by secondary electron emissions from impinging ions on the previous grids.

This was followed by the practical application and detailed instructions necessary for building the probe and associated circuitry. Materials were chosen to various requirements such as machinability, high temperature resistance, adequate conductivity, and availability. Next, the process for constructing the probe was outlined in detail to make the construction repeatable. Several jigs and methods were developed to ensure proper operation and ease of manufacturing for the individual parts.

A new programming environment was used to create a data acquisition scheme. This was coupled with circuitry designed to give adequate response while minimizing noise and electrical pickup. A simple user interface was developed to allow for rapid data acquisition and pre-processing.

Next, experiments were conducted to verify that the probe worked in accordance with the theory presented. Sample data was taken and analyzed resulting in preliminary results revealing an ion temperature much higher than was expected to be present. Distribution functions obtained indicate that the ion distribution fits very closely to a Maxwellian distribution function. This preliminary data shows that further investigation is necessary for determining ion heating processes occurring in the VTF plasma. In addition, as with many diagnostics, several improvements can be made.

6.2 Future Experiments

The GEA presented in this thesis is just a starting point for many new experiments for the VTF machine. First, the accuracy of the GEA readings can be increased for better results. Second, more data needs to be taken with several different plasmas and different radii of the device. Finally, an investigation of the ion heating process should be examined to determine the physics occurring in the VTF plasma.

The first step in improving the accuracy in the GEA is simply to build another tip and restore the operation of the probe. It should also be noted that the characteristic traces in Section 5.2 are somewhat noisy. This problem has been corrected by reducing the circuit interference and adding a digital filter in the acquisition program. Bench tests have been done to ensure that the noise has been reduced. However, it should be tested in the actual working environment once the new probe tip is installed and verified to be working. Another item to examine when building another tip would be to achieve a probe cross section such that $r_{probe} \geq \rho$. This

would allow for ion temperature to be examined instead of limiting the results to ion temperature parallel to the magnetic field. The difficulty lies in the deformation of the grids when they are heated. When the grid is slightly heated some deformation can occur which can cause a grid to become incident on an adjacent grid resulting in probe tip failure. A method for ensuring adequate grid spacing with a larger unsupported area must be resolved.

Another item, which would lead to better diagnostic performance, is the characterization of the floating potential at the same port location as the GEA. Floating potential has only been measured at the mid-plane in previous experiments. A plot of floating potential versus major radius would be useful for determining the entrance grid potential based upon the probes radial position. This would be used to achieve the proper matching of the entrance grid voltage to the plasma to achieve a more accurate distribution function as mentioned in Jones (1976). Jones showed that this could lead to significant errors in temperature measurements with a GEA.

Several other simple modifications could be made to the existing probe to aid in data collection. A mechanism for radially scanning the probe during a plasma shot would be convenient for the operator. Currently to change the position for measurement, the operator must enter the cell between shots and manually position the probe. An automated device for positioning the probe either during or between plasma shots would allow fast and accurate data collection. The back plate of the probe structure was left unoccupied to allow for a mechanism to be mounted such as a motor drive which could even be controlled by the operator from the control room.

Another useful modification would be an alteration of the LabView processing subroutine. The current screen output and data file could be modified to include a distribution function and temperature reading. LabView contains the ability to do the mathematical manipulations but the subroutines need to be written. This would allow the operator to view the desired data almost instantaneously without requiring several minutes of manipulation to achieve the same effect.

Furthermore, this thesis involves the design and construction of the gridded energy analyzer. The device was only taken to the point of operation to show that the GEA worked in the VTF. For proper scientific consideration many more experiments need to be done. Data should be taken and analyzed at several different major radii in the VTF. In addition, several different plasma shots should be run with varying toroidal and vertical fields. Various beam currents and microwave plasmas should be examined. Only then will future researchers have a better understanding of the VTF plasma generation capabilities.

Along with collecting data with the GEA from various different plasmas in the VTF, a future investigation of the ion heating process is warranted. Kindel and Kennel (1971) showed that when electron and ion temperatures were comparable excitation of the ion acoustic wave was greatly enhanced. Once this enhancement occurs Landau Damping of the ion acoustic wave could lead to increased heating of the ions. Research on this phenomena in VTF is still in progress (Riddolls, 1996). Before these preliminary results, it was believed that $T_e > T_i$; however, it appears the assumption may not be correct for all VTF plasmas. Should these results prove to be true, it could impact many experiments and theories regarding the VTF plasma.

As can be seen, there are many research opportunities available to pursue with the GEA. The GEA designed in this thesis provides another diagnostic for examining the physics of the VTF plasma. It is the hope of the author that this thesis will provide a strong basis for future research by others.

Bibliography

D. N. Arion and R. F. Ellis, *New Electron Energy Analyzer for Magnetized Plasmas*, Rev. Sci. Instrum. **53**, 1032 (1982).

P. Beiersdorfer, V. Decaux, S. R. Elliott, K. Widmann, and K. Wong, *Temperature of the Ions Produced and Trapped in an Electron-Beam Ion Trap*, Rev. Sci. Instrum. **66**, 303 (1995).

D. Bohm, E. H. S. Burhop and H. S. W. Mossey, *Characteristics of Electrical Discharges in Magnetic Fields*, McGraw-Hill, New York, 1949.

F. Chen, *Introduction to Plasma Physics and Controlled Fusion*, Plenum Press, 1984.

R. W. Gould, *Excitation of Ion-Acoustic Waves*, Phys. Rev., **136**, A991 (1964).

I. H. Hutchinson, *Principles of Plasma Diagnostics*, Cambridge University Press, Cambridge, 1987.

R. Jones, *Optimization and Performance of Electrostatic Particle Analyzers*, Rev. Sci. Instrum. **49**, 21 (1976).

N. Kaya, *New Technique for Direct Measurement of Electron Temperature*, Rev. Sci. Instrum. **53**, 1049 (1982).

J. M. Kindel and C. F. Kennel, *Topside Current Instabilities*, J. Geophys. Res., **76**(13), 3055 (1971).

Yu. E. Kolyada, E. A. Kornilov, Ya. B. Fainberg, and V. S. Kiyashko, *Ion Heating and Beam Trapping in the Interaction of High Current Electron Beam with a Plasma in a Magnetic Mirror*, Technical Physics, **22**, 47 (1977).

N. Krall and A. Trivelpiece, *Principles of Plasma Physics*, McGraw-Hill, Inc., New York 1973.

M. C. Lee, R. J. Riddolls, K.D. Vilece, N. E. Dalrymple, M. J. Rowlands, D. T. Moriarty, K. M. Groves, M. P. Sulzer, and S. P. Kuo, *Laboratory Reproduction of Arecibo Experimental Results: HF Wave-enhanced Langmuir Waves*, Geophys. Res. Lett., **24**, 115 (1997).

A. T. Lin and C. Lin, *Nonlinear Penetration of Upper-Hybrid Waves Induced by Parametric Instabilities of a Plasma in an Inhomogeneous Magnetic Field*, Phys. Rev. Lett. **47**, 98 (1981).

D. T. Moriarty, *Design and Construction of the Versatile Toroidal Facility for Laboratory Simulation of Ionospheric Plasmas*, MIT Department of Electrical Engineering and Computer Science Bachelor's Thesis, 1990.

D. T. Moriarty, *Electron Cyclotron Range of Frequencies Propagation in Critically Dense Cold Magnetoplasmas*, MIT Nuclear Engineering Department Master's Thesis, 1992.

D. T. Moriarty, *Laboratory Studies of Ionospheric Plasma Processes with the Versatile Toroidal Facility*, MIT Nuclear Engineering Department Doctoral Thesis, 1996.

Massachusetts Institute of Technology, *Plasma Laboratory 22.69 Class Notes*, (Spring 1997).

D. R. Nicholson, *Introduction to Plasma Theory*, John Wiley and Sons, Inc., New York, 1983.

Physics Through the 1990s: Plasmas and Fluids, National Academy Press, Washington, D.C., 1987.

R. J. Riddolls, M. C. Lee, D. T. Moriarty, S. M. Murphy, D. Pooley, *Laboratory Study of Anti-Stokes Langmuir Waves in A Magnetized Plasma,* Proceedings, 22nd IEEE ICOPS, Madison, WI, 1995.

R. J. Riddolls, *Laboratory Experiments on RF and Electron Beam Excited Plasma Waves,* Department of Electrical Engineering and Computer Science paper, 1996.

J. R. Roth and M. Clark, *Analysis of Integrated Charged Particle Energy Spectra From Gridded Electrostatic Analyzers*, Plasma Phys. **11**, 131 (1969).

S. Stephanakis and W. H. Bennett, *Electrostatic Energy Analyzer for Studying Gas-Focused Electron Beams and Their Background Media*, Rev. Sci. Instrum. **39**, 1714 (1968).

R. L. Stenzel, R. Williams, R. Agüero, K. Kitazaki, A. Ling T. McDonald, and J. Spitzer, *Novel Directional Ion Energy Analyzer*, Rev. Sci. Instrum. **53**, 1027 (1982).

R. L. Stenzel, W. Gekelman, N. Wild, J. M. Urrutia, and D. Whelan, *Directional Velocity Analyzer for Measuring Electron Distribution Functions in Plasmas*, Rev. Sci. Instrum. **54**, 1302 (1983).

A. Y. Wong, R. W. Motley, and N. D'Angelo, *Landau Damping of Ion Acoustic Waves in Highly Ionized Plasmas*, Phys. Rev., **133**, A436 (1964).

N. Yajima,Y. Kawai, and K. Kogiso, *A Heating Mechanism of Ions Due to Large Amplitude Coherent Ion Acoustic Wave*, Journal of the Physical Society of Japan, **45**, 1985 (1978).

T. F. Yang, P. Liu, and Q. Z. Zu, *Determination of Ion Temperature with Single and Triple Langmuir Probes*, Submitted to Rev. Sci. Instrum., (1994).

Appendix A. Materials List

Sauereisen Cements
160 Gamma Drive
Pittsburgh, PA 15238-2989
phone: (412) 963-0303
fax: (412) 963-7620

Item No.	Description	Unit Price
7	Insa-lute Hi Temp Cement (paste) approximate shelf life is 6 months	19.95

McMaster-Carr
P.O. Box 440
New Brunswick, NJ 08903-0440
phone: (908) 329-3200
fax: (908) 329-3772

Item No.	Description	Unit Price
8802K11	rigid mica wafers .004"x2"x4"	.93
87175K95	Alumina four bore tube 36" ID .031" OD .188"	27.37
8975K148	Aluminum 1"x6"x72"	139.32
8982K24	Angle Aluminum 1 1/2"x3/16"x96"	19.76
8954K41	Brass 3/16"x4"x72"	46.16
89935K61	Stainless steel tubing 12" OD.219" ID.199"	12.80
2407T79	Swivel caster w/brake 4"	13.22
2407T94	Caster 4"	7.66
89895K25	Stainless steel tubing 5 ft OD 5/16" .035" thick	44.16

Other Items used

Teflon 3/8" thick
stainless steel rods 3/4" DIA, 5 ft
stainless steel rods 9/16" DIA, 5 ft
linear bearings 3/4" ID 1 1/8" OD
Kepco BOP-500M programmable power supply
Sorensen High Voltage Power supply
Burr-Brown Isolation Amplifier Model 3456A
Huntington vacuum bellows 19" throw, 25" maximum, .62" ID
2 3/4" to 1 1/3" reducing flange
2 3/4" vacuum blank
2 3/4" vacuum Tee joint
2 3/4" ion gauge electrical feed through

Appendix B. Technical Drawings

Important information about drawings

1. Tolerances are as follows:

    A. Dimensions marked to the thousandth have a tolerance of 0.001 mm.

    B. Dimensions marked to the hundredth have a tolerance of 0.01 mm.

    C. Dimensions marked to the tenth have a tolerance of 0.1 mm.

    D. Dimensions without decimals have a tolerance of 5 mm.

2. All plates are should be machined with the reference for all dimensions marked off from the midpoint of the plate. This starting point allows for proper alignment of all the bearings and rods so that no binding occurs.

3. It is also important to note that the outside dimensions of the plates are not critical to any operation and as such that is why the tolerances are high.

B.1 Back Plate Machine Drawing

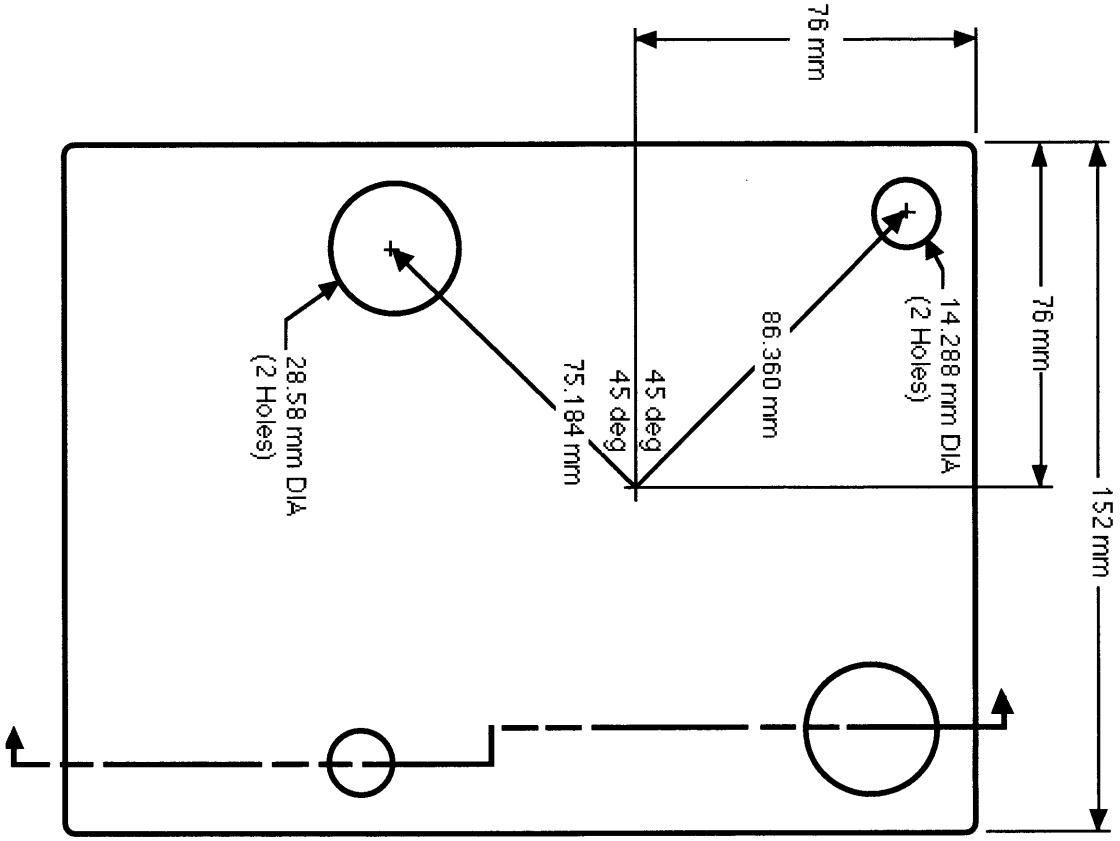

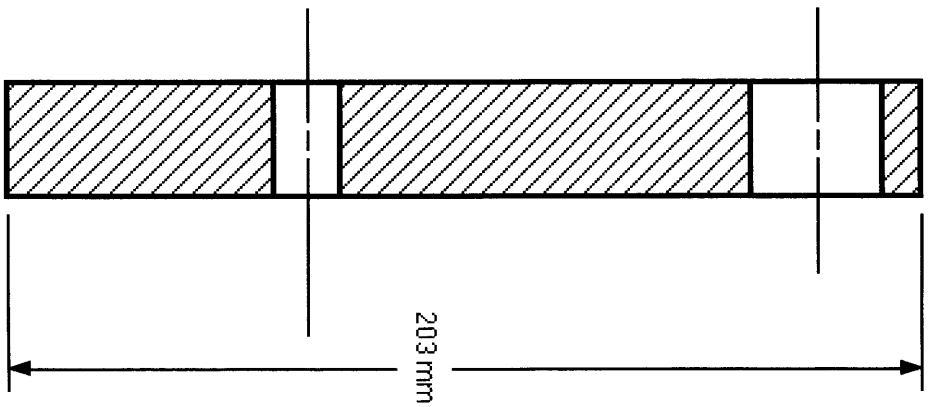

B.2 Support Plate Machine Drawing

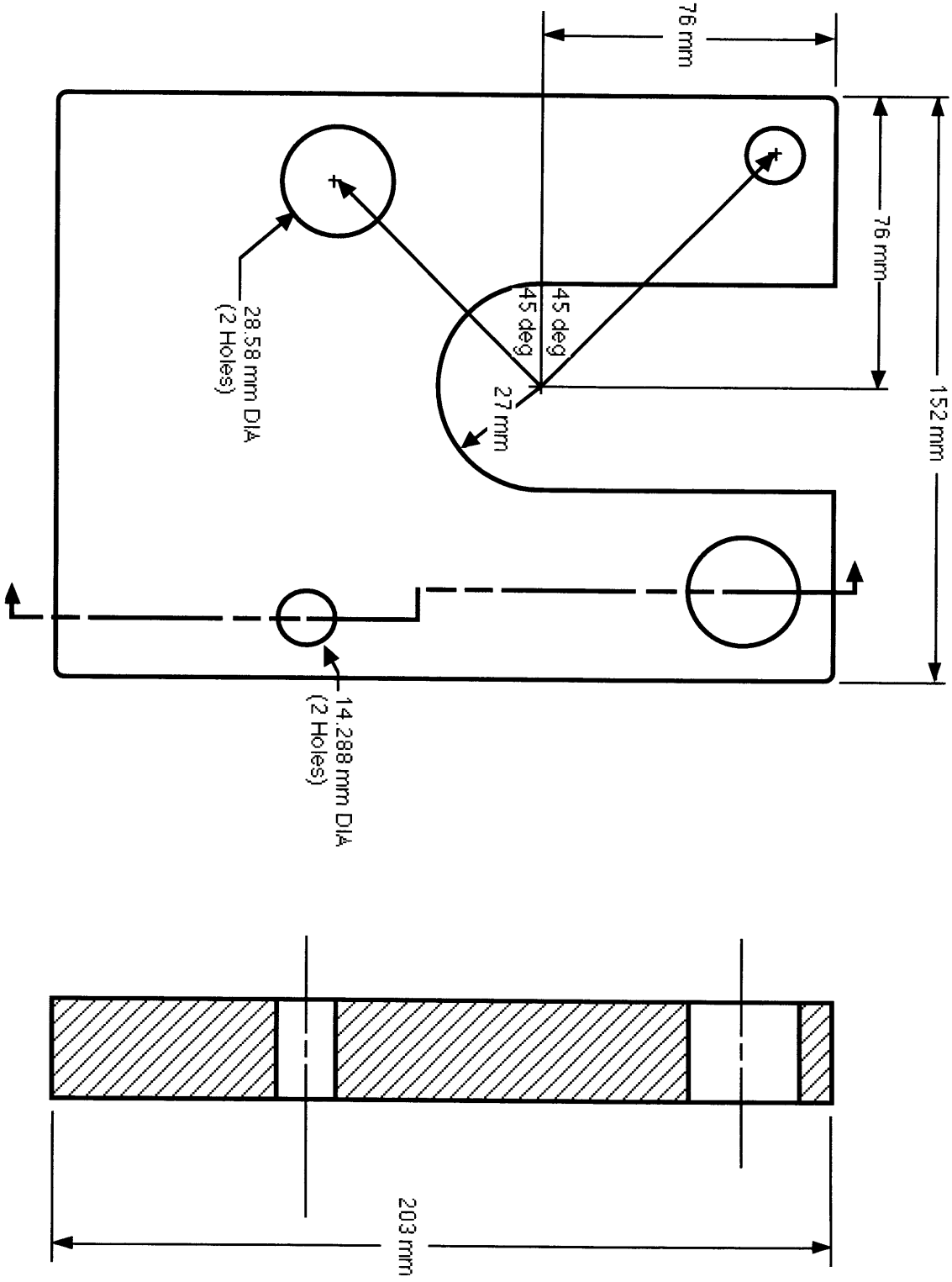

B.3 Mounting Plate Machine Drawing

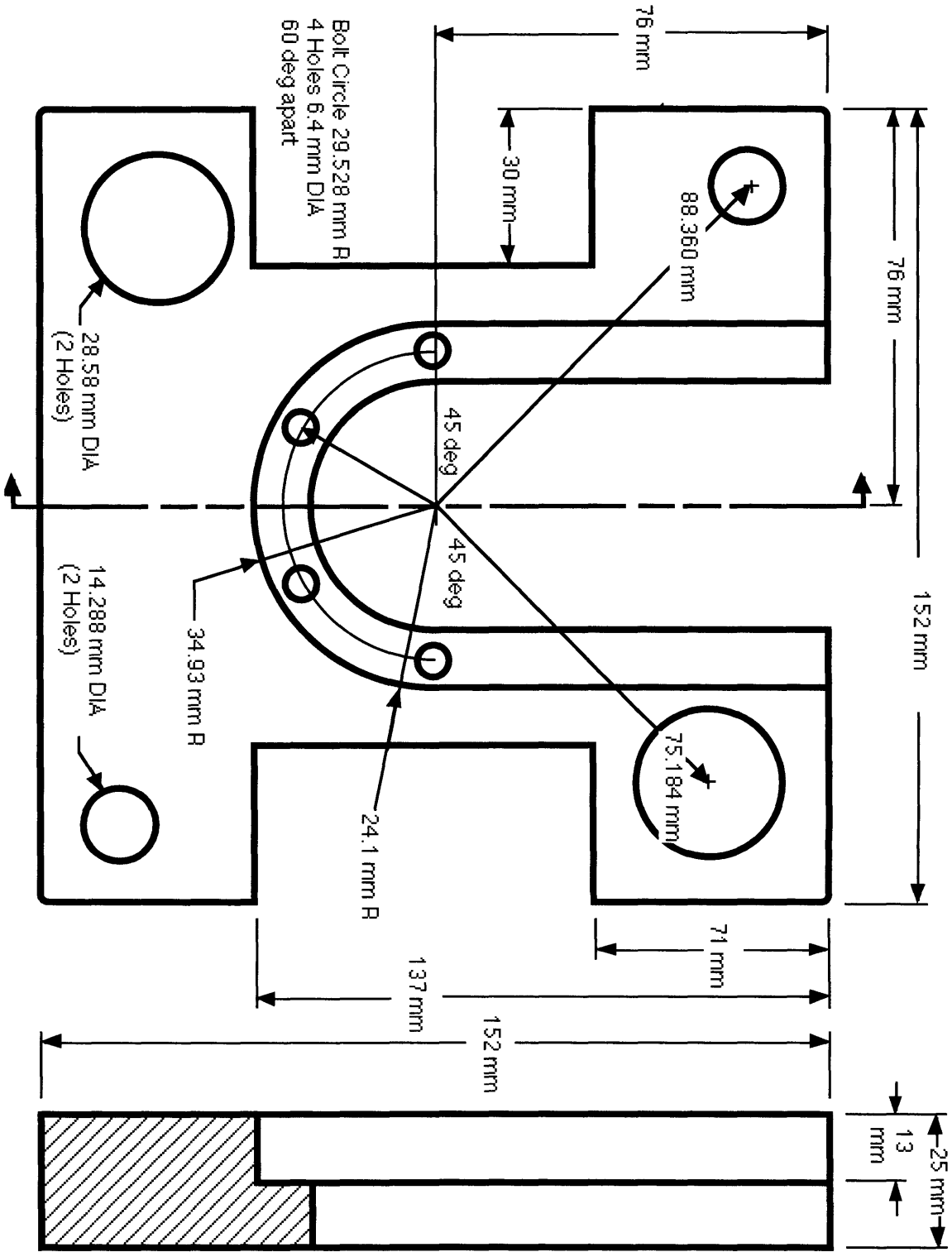

B.4 Front Carriage Plate Machine Drawing

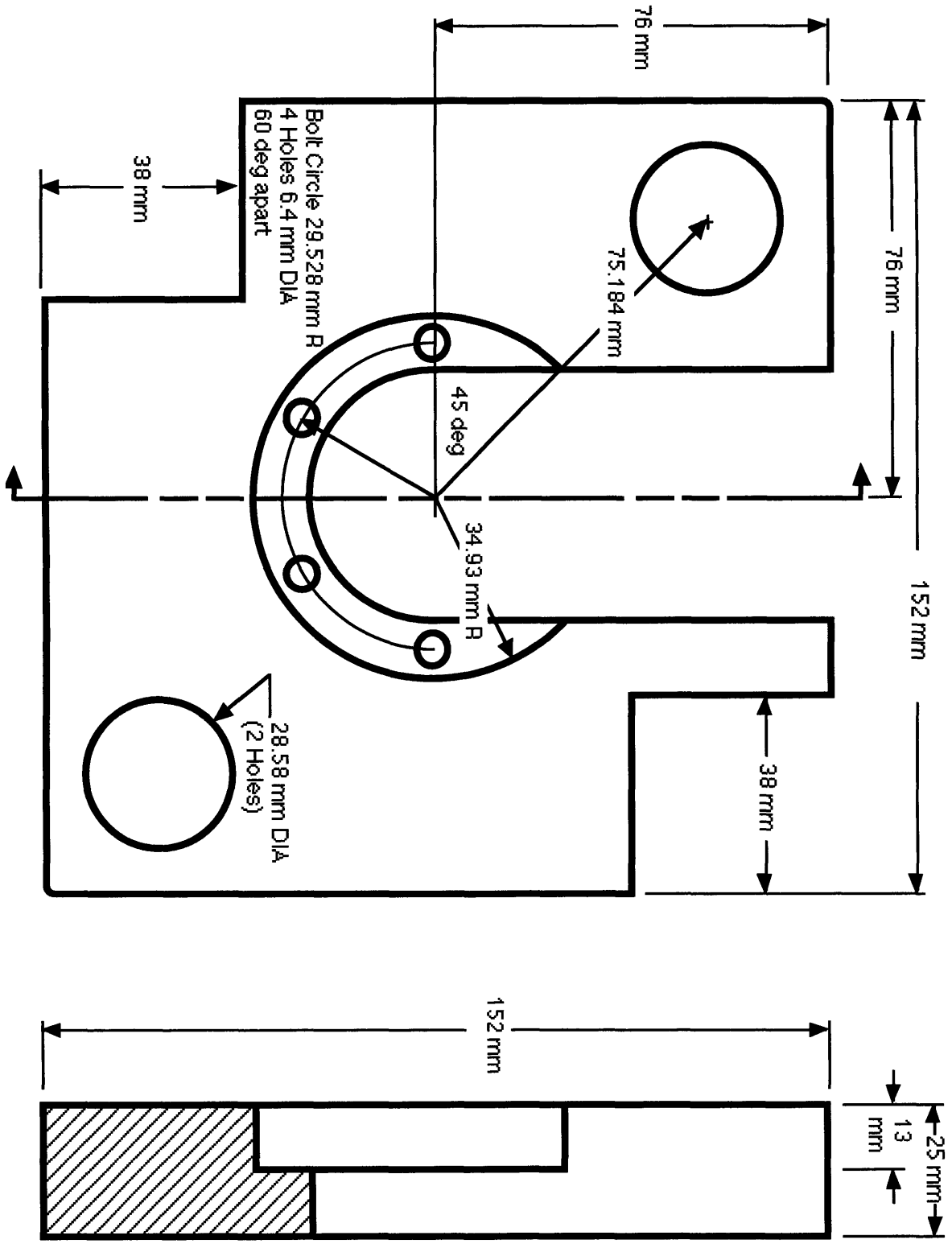

B.5 Rear Carriage Plate Machine Drawing

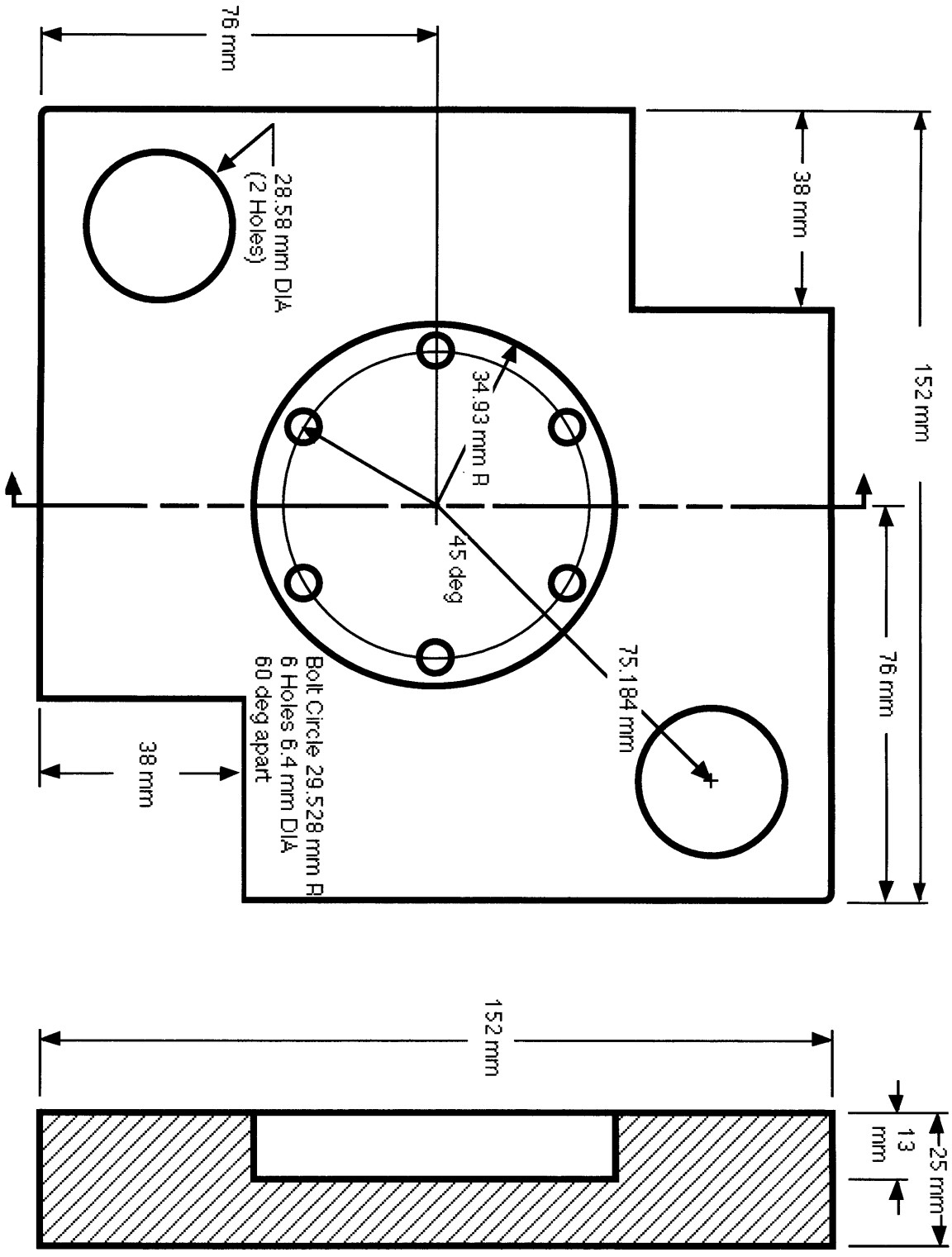

Appendix C. LabView Program

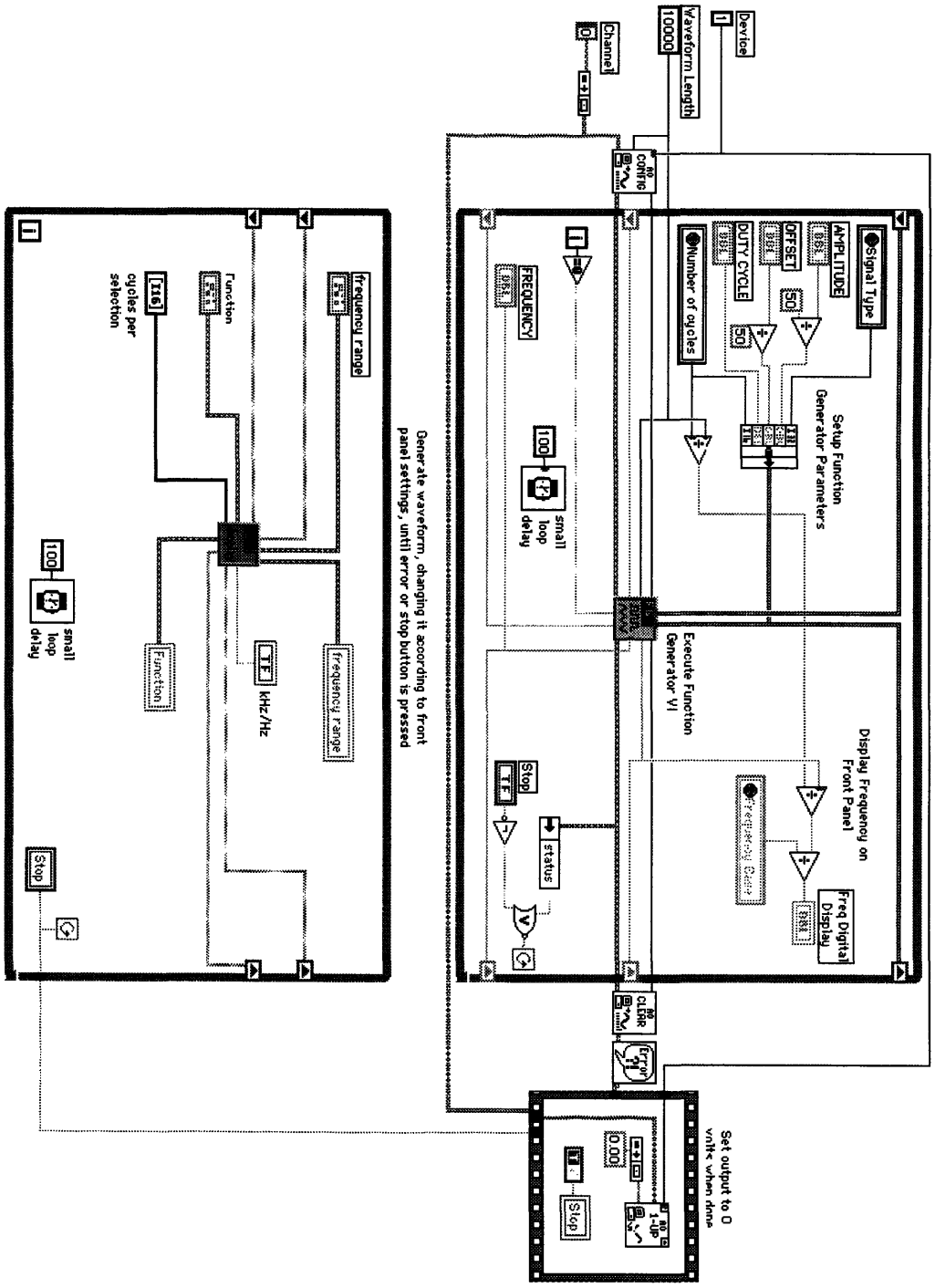

Figure 43. GEA Function Generator Program

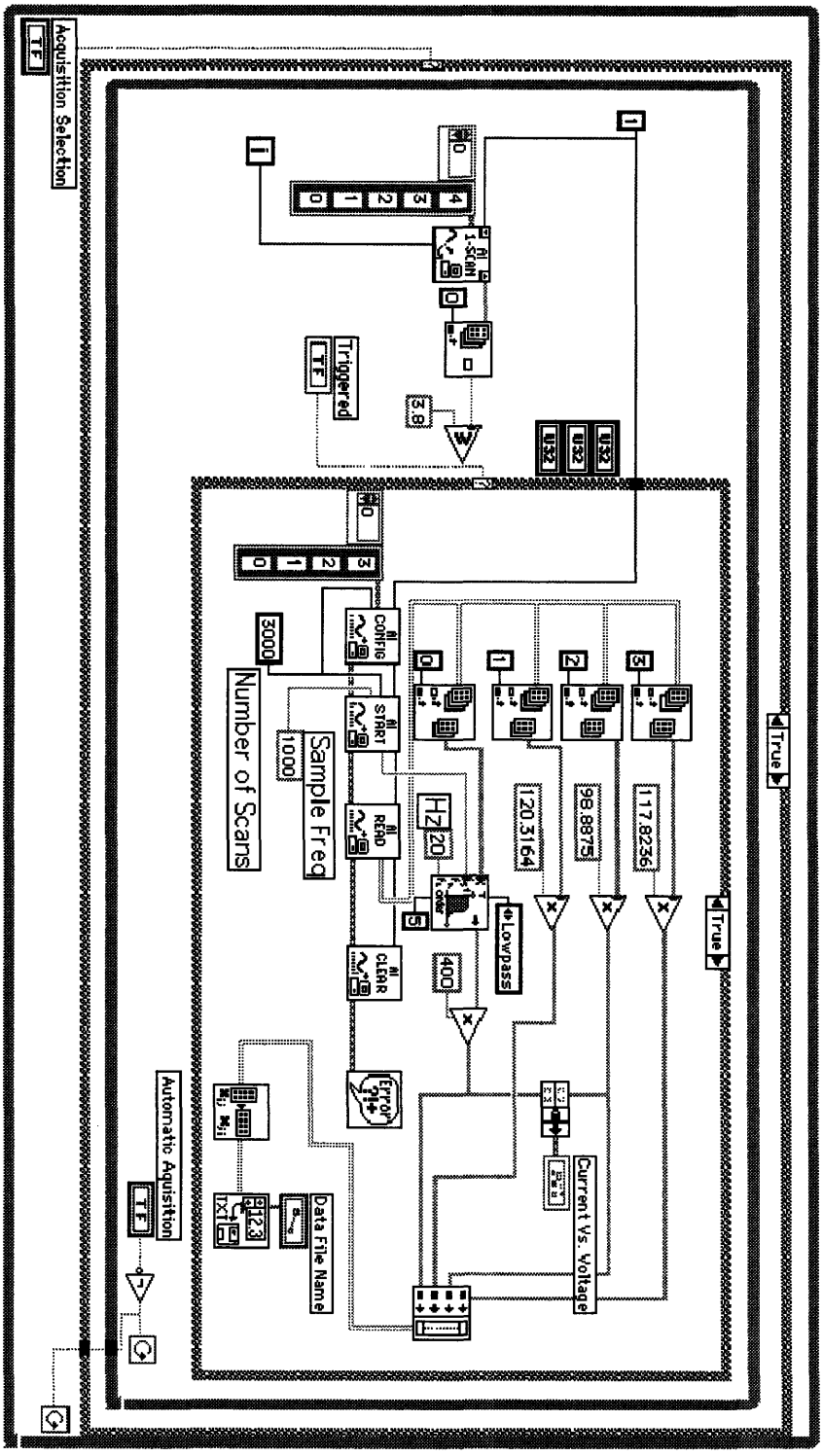

Figure 44. GEA Main Acquisition Program

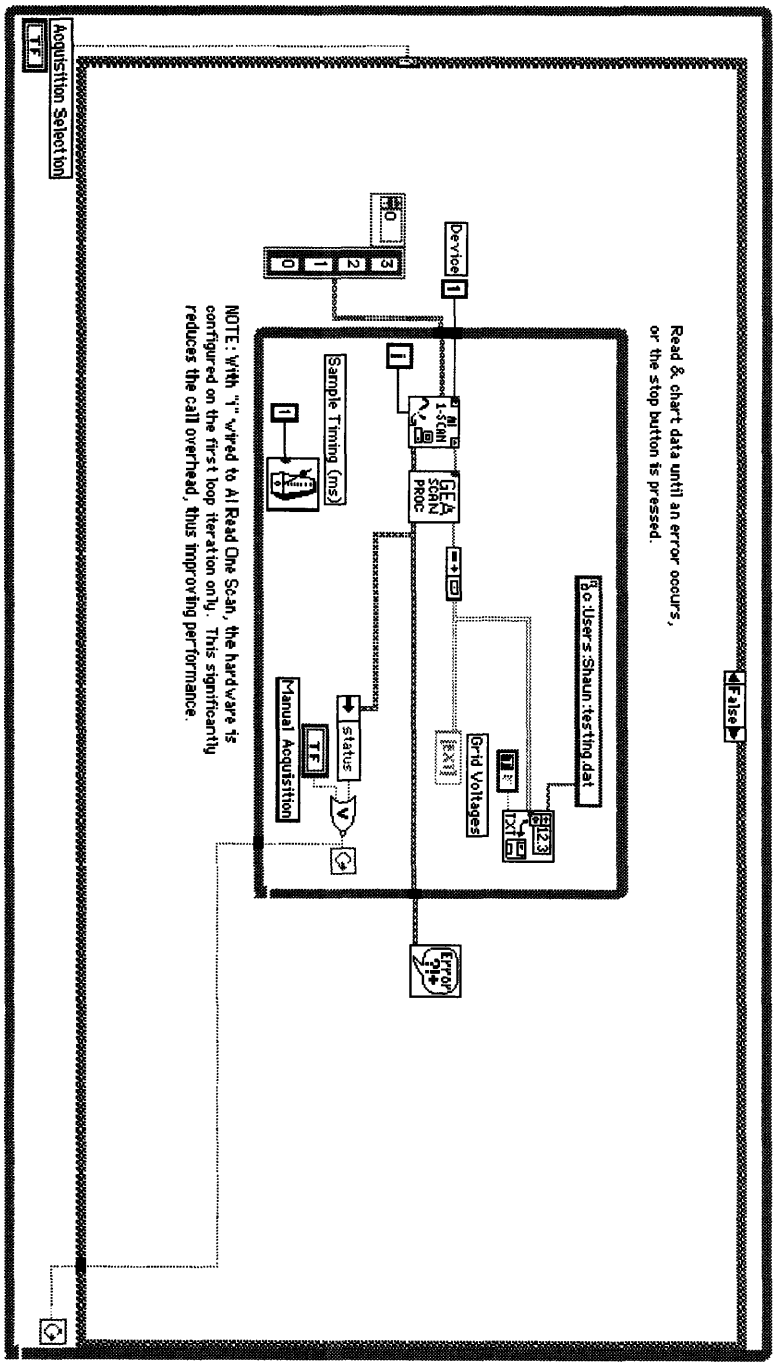

Figure 45. GEA Manual Acquisition Program

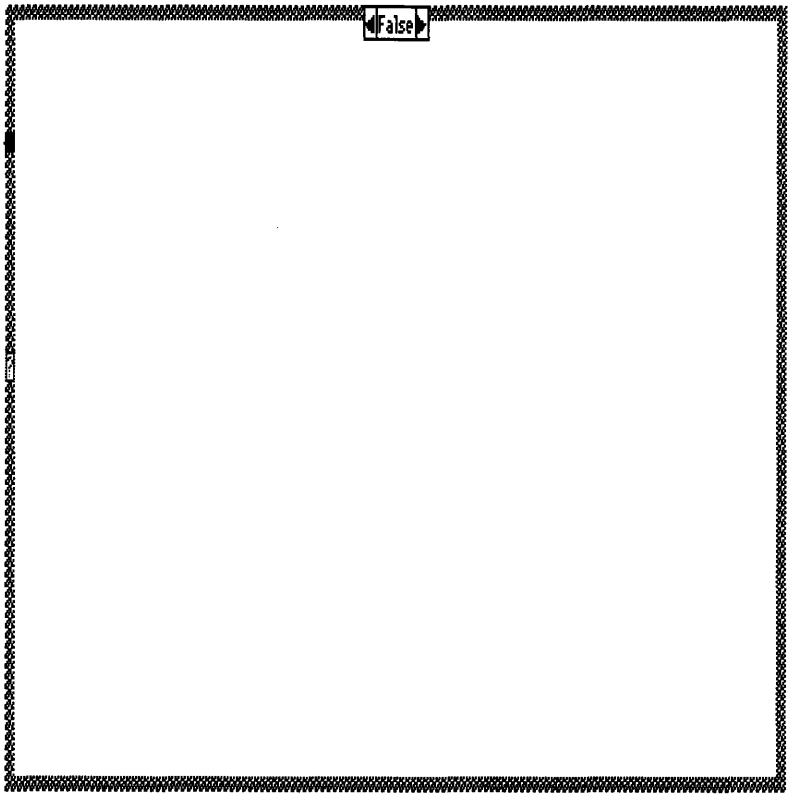

Figure 46. GEA Not Triggered Routine